ABSTRACT

POTENTIALLY ACTIVE FAULTS IN CENTRAL MONGOLIA

By

Tiffany Guiltinan

January 2015

The activity of the Ereen Uul fault and the Sanglin Dalai Nurr fault in central Mongolia has not been studied in detail. The Erren Uul fault is a normal fault located 45 km southeast from Harhorin and the Sanglin Dalai Nurr fault is a right-lateral strike-slip fault located 30 km south of Harhorin next to the Hangay Mountains. Remote sensing and field observations were used to refine a map by the Mongolian Geologic Survey at a scale of 1:1,000,000 to a scale of 1:100,000. This new map covers an area of 8,072 km^2. The basin asymmetry factor, stream length-gradient index, and hypsometric curves were developed for basins adjacent to these faults. These geomorphic indices along with the refined map were used to conclude that the Ereen Uul and Sanglin Dalai Nurr faults are active.

POTENTIALLY ACTIVE FAULTS IN CENTRAL MONGOLIA

A THESIS

Presented to the Department of Geological Sciences

California State University, Long Beach

In Partial Fulfillment

of the Requirements for the Degree

Master of Science in Geology

Committee Members:

Thomas Kelty, Ph.D. (Chair)
Lora Stevens-Landon, Ph.D.
Nate Onderdonk, Ph.D.

College Designee:

Robert D. Francis, Ph.D.

By Tiffany Guiltinan

B.S., 2009, California State University, Long Beach

January 2015

ProQuest LLC.
789 East Eisenhower Parkway
P.O. Box 1346
Ann Arbor, MI 48106 - 1346

ACKNOWLEDGEMENTS

I just wanted to say thank you for everyone who helped out with this thesis. A special thanks goes out to Roland and Debra Sauermann, who funded my plane tickets and field expenses. This project has been a great learning experience for me and it would not have been possible without your support.

I also want to thank both of my field assistants, Liz Vasquez and Gankhuyag Jadamaba. Liz, thank you for your help taking measurements and thank you for your sense of humor that made this trip so much fun. Gankhauyag, thank you for translating for us and for all your help in the field!

Thank you to my advisor, Tom Kelty, for setting me up with this great project and taking me on as a student. I would also like to thank my committee members, Nate Onderdonk and Lora Stevens, for their thoughtful comments.

Thank you to our driver, Amgalan, for taking us to all our field locations. It was really nice getting to know you.

Thanks to Paul Day for showing me how to use the ENVI software program and helping me create false color images before we left for the field.

Ulzii, thank you for setting up all the connections in Mongolia, you set us up with great people.

Thank you Eric for showing me how to use different tools in ArcGIS it was really helpful. I also wanted to thank you for all of your support. I would have not finished without you.

The thesis is complete!!! Thank you all again!!! =)

TABLE OF CONTENTS

Page

CHAPTER Page

LIST OF TABLES

TABLE Page

LIST OF FIGURES

FIGURE Page

FIGURE Page

FIGURE Page

FIGURE Page

FIGURE Page

CHAPTER 1

INTRODUCTION

Statement of Purpose

Mongolia has a complex geologic history and there are on-going debates about its development (e.g., Mossakovsky et al., 1994; Didenko et al., 1994; Buchan et al., 2001; Sengör et al., 1993). Mongolia has been extensively mapped at a scale of 1:500,000 (Byamba, 1990); however, more detailed assessments of the structural development are lacking. This study uses remote sensing, field data, and geomorphological observations to describe and map the northern section of the Övörhangay province and along the southern border of the Arhangay province in central Mongolia with focus on the Sangiin Dalai Nuur and Ereen Uul faults. The objectives of this study were to (1) create a geologic map of this area at a scale of 1:100,000, (2) determine if these faults are active, and 3) if active, describe their most recent movement.

Physiography and Climate

Mongolia is a landlocked country located between Russia and China (Figure 1). It has an average altitude of 1,580 meters above mean sea level. This study was completed in the northern section of the Övörhangay province and along the southern border of the Arhangay province, in central Mongolia. The area is characterized by rolling hills, rivers and flood plains. Mongolia can have extreme weather conditions. Winter starts in early November and lasts until March with an average temperature of

-20° C. The summer months are from the end of May to August, with an average temperature of 20° C (www.weather-and–climate.com). Figure 2 illustrates the average monthly minimum and maximum temperatures in Saikhan-Ovoo, which is located 120 km south of the field area.

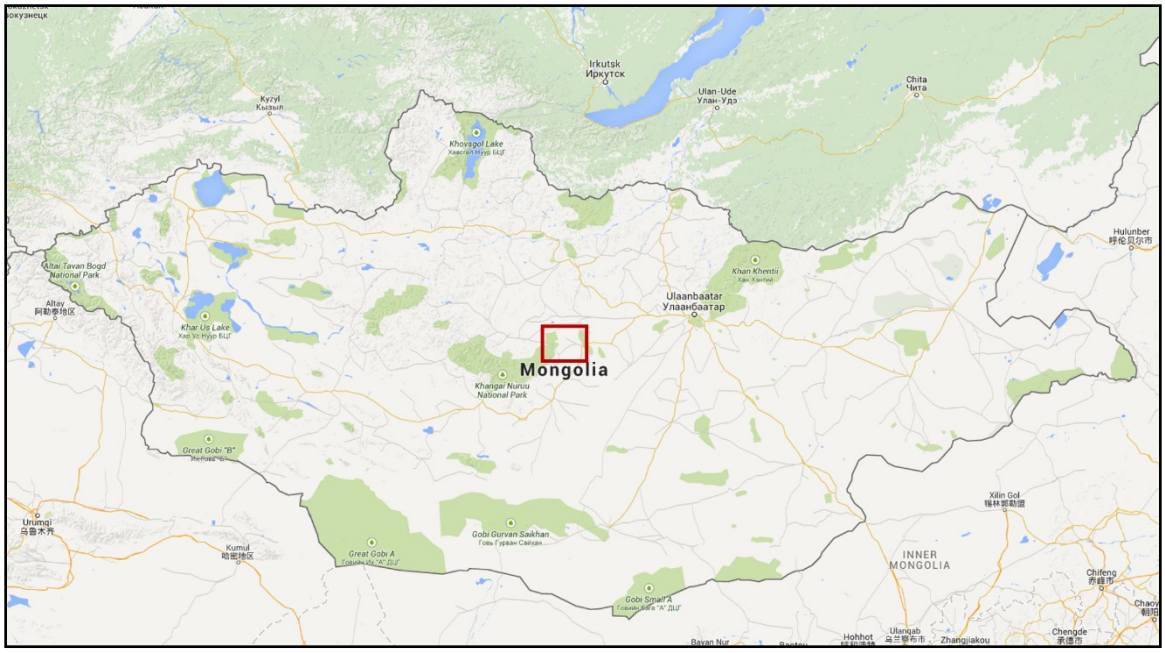

FIGURE 1. Map of Mongolia with the study area outlined in red.

Precipitation varies largely by region and season. Figure 3 shows a graph of the average monthly precipitation throughout the year in the vicinity of the field site. The weather can quickly change.

FIGURE 2. The average minimum and maximum temperatures in Saikhan-Ovoo, Mongolia, located 120 km south of the field area. Figure modified from www.weather-and-climate.com.

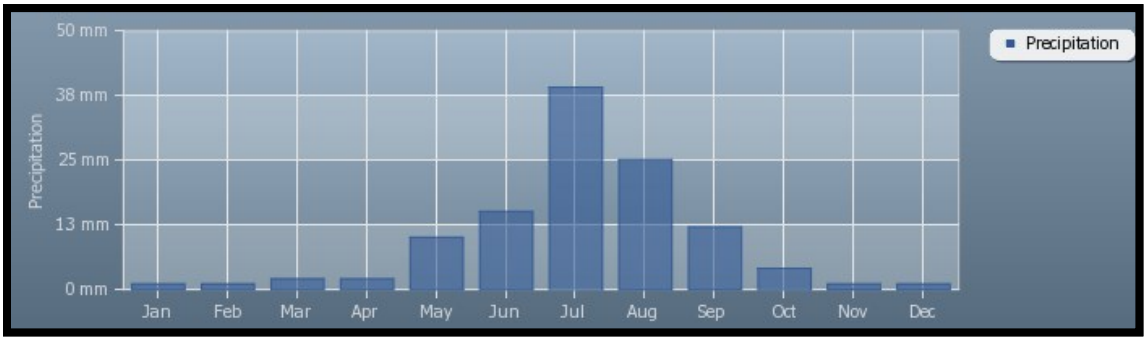

FIGURE 3. Average precipitation as rain or snow in Saikhan-Ovoo. Mongolia. Figure modified from www.weather-and-climate.com.

CHAPTER 2

REGIONAL GEOLOGY

The Central Asian Orogenic Belt

Numerous mountain ranges characterize the physiography of central and western Mongolia. These ranges include the Mongolian Altai Mountain range, which is oriented approximately N 30°W; the Gobi Altai Range in central Mongolia, which is oriented approximately N70°W; and the Hangay Range, which is located in central Mongolia and is oriented approximately N 50° W. Together these mountain ranges compose part of the Central Asian Orogenic Belt (CAOB). Jishun and Tingyu (1989) describe the CAOB as one of the most complicated mountain belts because of its geologic history. The complex history of the CAOB has created an ongoing debate over its formation. Contributing to the confusion surrounding the geologic history of the CAOB is the numerous names used in the literature. These include the "Altaid Tectonic Collage" (Şengör and Natal'in, 1996; Şengör et al., 1993) the Mongolian-Hinggan Orogenic Belt (Jishun and Tingyu, 1989), and the Central Asian Orogenic System.

Regardless of the details of formation, the CAOB is one of the longest lived and largest accretionary orogens in the world (Wilhem et al., 2012). The CAOB is located between the Siberian craton to the north and the Tarim and North China cratons to the south (Jahn, 2004; Jong et al., 2009; Xu et al., 2013; Figure 4). The CAOB is composed of island arcs, accretionary complexes, passive continental margins, and Precambrian

continental blocks (Badarch et al., 2002; Didenko et al., 1994; Jahn, 2004; Kröner et al., 2010; Mossakovsky et al., 1994; Xiao et al., 2003; Xu et al., 2013).

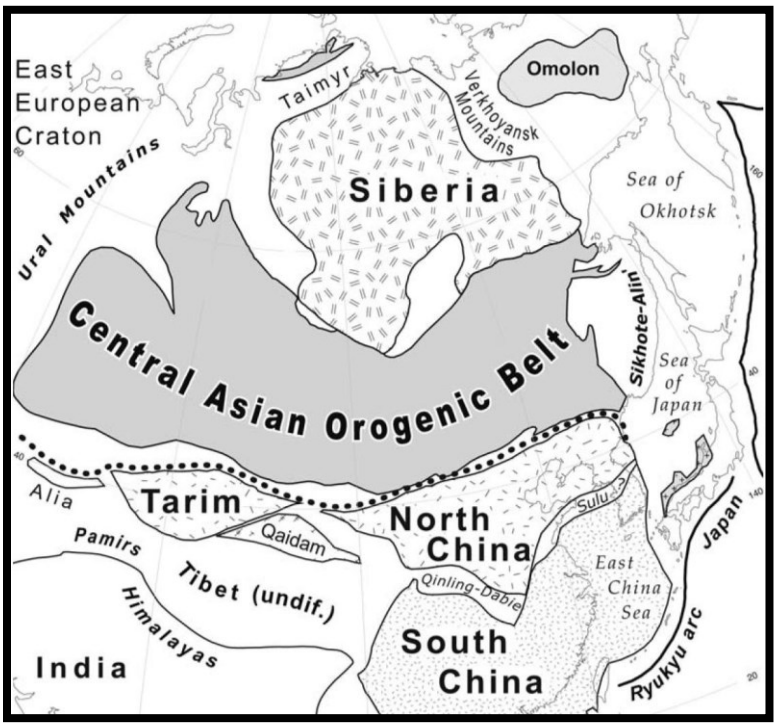

FIGURE 4. Location of the CAOB in relation to the Siberian craton to the north and the Tarim and North China cratons to the south. This reconstruction is during the Mesozoic Era. Image modified from (Jong et al., 2009).

The CAOB is divided into the northern domain and southern domain, which are separated by the Main Mongolian Lineament. The northern domain is composed of granitic and metamorphic rocks from the Precambrian and Lower Paleozoic Eras. The geologic units include ophiolites from the Neoproterozoic, island-arc volcanics from the Lower Paleozoic, meta-sediments from the Devonian to Carboniferous, and volcanic-plutonic rocks from the Permian (Badarch et al., 2002). The southern domain is *composed of Paleozoic rocks, which are arc-related volcanics and volcaniclastic rocks*

with fragments of ophiolites and serpentinite mélanges (Badarch et al., 2002). This study is centered north of the Main Mongolian Lineament (Figure5).

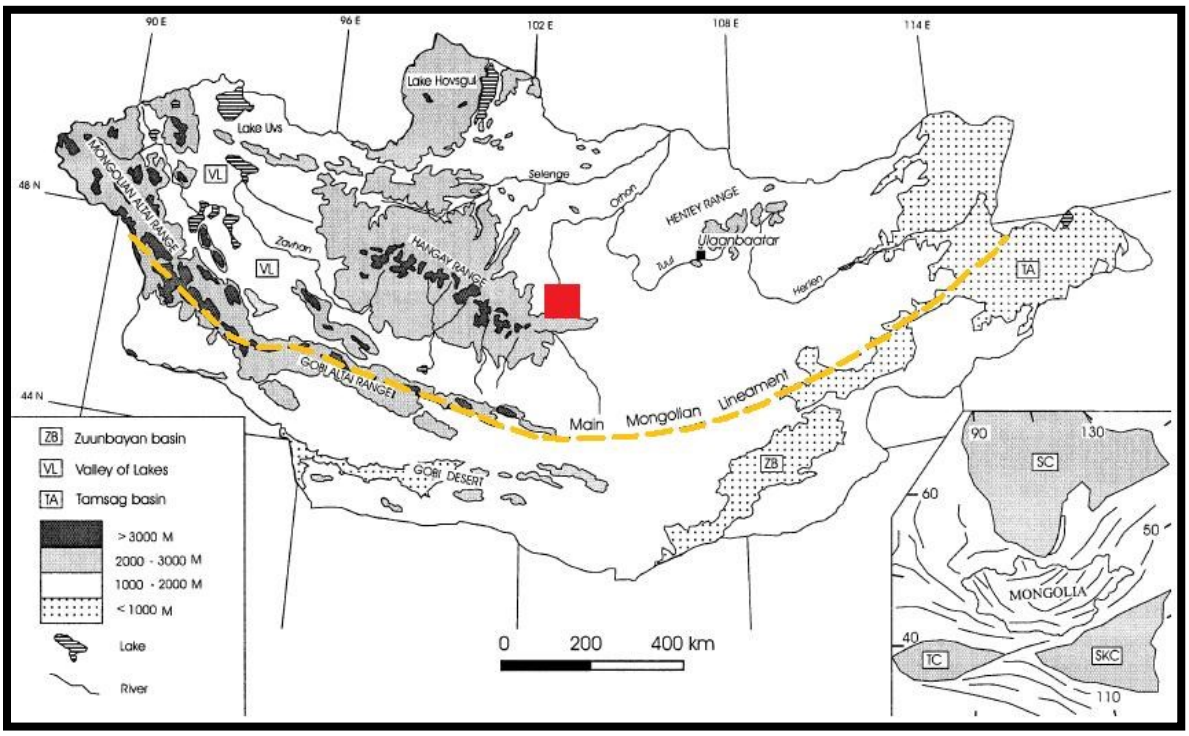

FIGURE 5. Map of the CAOB showing the Main Mongolian Lineament (dashed yellow line). Field area for this thesis is within the Hangay Hentey basin west of the Hangay range and is marked by a red square. Image modified from (Badarch et al., 2002).

Formation of Mongolia

There are conflicting geologic interpretations regarding the tectonic development and formation of the CAOB in Mongolia and surrounding regions. Two scenarios are considered to be the most plausible and include (1) the development of Mongolia by continuous ocean-ward migration of a single subduction zone and strike-slip fault stacking to create the entire CAOB (Şengör and Natal'in, 1996; Şengör et al., 1993) and (2) the closure of a small ocean by multiple subduction zones resulting in the abduction

of ophiolites and accretion of island arcs and microcontinents suturing to the Siberian and China cratons (Badarch et al., 2002; Buchan et al., 2001; Didenko et al., 1994; Mossakovsky et al., 1994; Windley et al., 2007; Xiao et al., 2003).

Scenario One: Long Single Subduction Zone

Şengör and Natal (1996) and Şengör et al. (1993) argue that Mongolia formed from an island arc system, with a single subduction zone that exceeded over 5,000 km in length and that was split by a series of strike-slip faults. The island arc system was amalgamated onto the margins of the Siberian craton. Figures 6 through 8 display Şengör and Natal'in's (1996) model of the CAOB's (referred to as the Altaids) creation during the Late Cambrian to Early Carboniferous. Şengör and Natal'in (1996) suggest that the CAOB formed from material common to present day subduction accretion complexes including immense plutons mostly from magmatic arc origin. Şengör and Natal'in (1996) also mention that it is difficult to find geologic evidence that outline the continental scale structures to form these subduction accretion complexes. In particular, ophiolites cannot be used to outline tectonic units because they are located throughout the basement of the CAOB structure. Paleo-magnetic data is not readily available, so Şengör and Natal'in (1996) use magmatic fronts as structural markers to reconstruct the units of the CAOB. These magmatic fronts display evidence of strike-slip fault stacking, which led to the idea that the CAOB is mostly composed of a collage of disrupted pieces of a single arc that is bounded by strike-slip faults. Figure 9 illustrates a generalized map of the CAOB and the surrounding cratons.

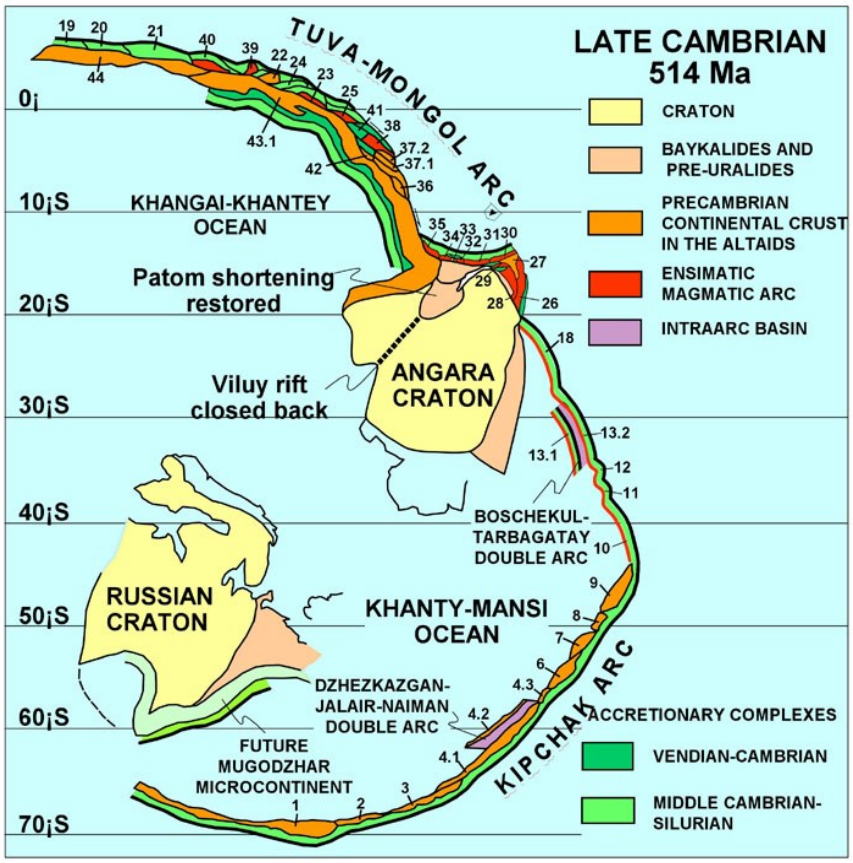

FIGURE 6. Late Cambrian reconstruction of the CAOB. Image modified from (Şengör and Natal'in, 1996).

The Tuva-Mongol Massif surrounds the Hangay Hentey basin. The massif is believed to have been a long linear strip that connected with the Siberian craton in the Late Proterozoic (Şengör et al., 1993; Figure 8). A subduction zone is postulated to have

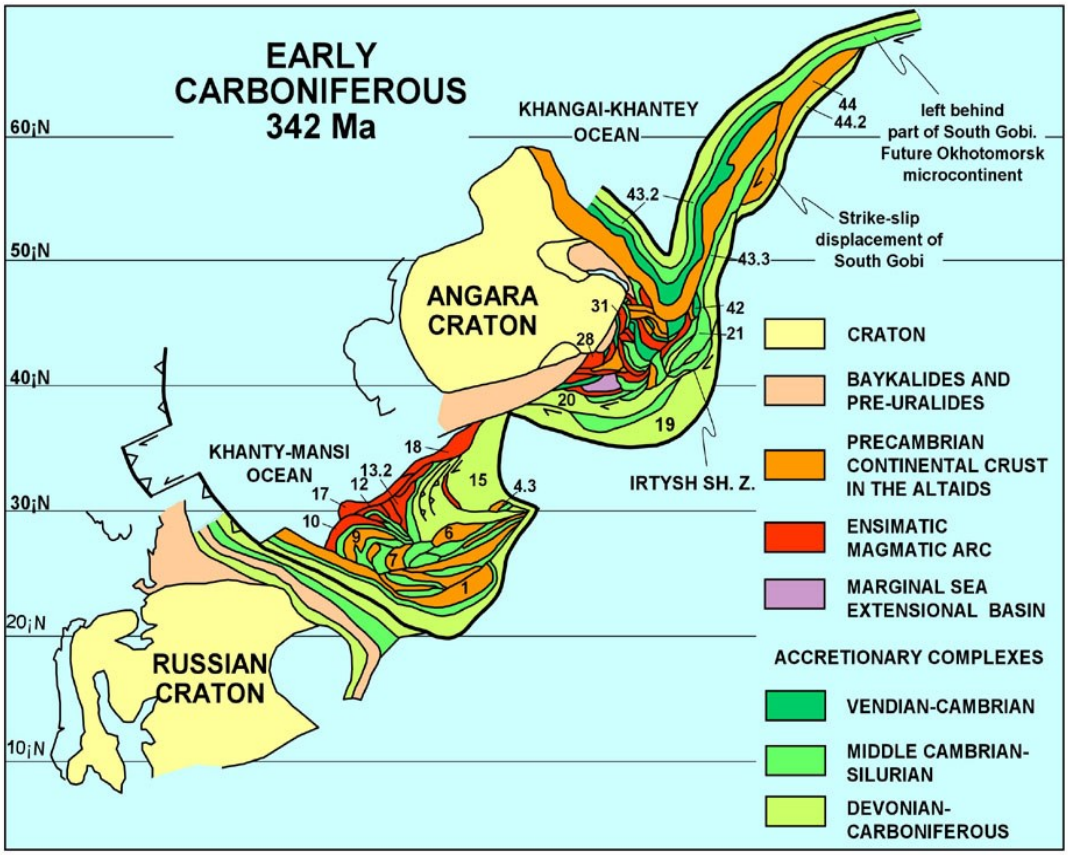

FIGURE 7. Reconstruction of the CAOB in the Early Carboniferous. Image modified from (Şengör and Natal'in, 1996).

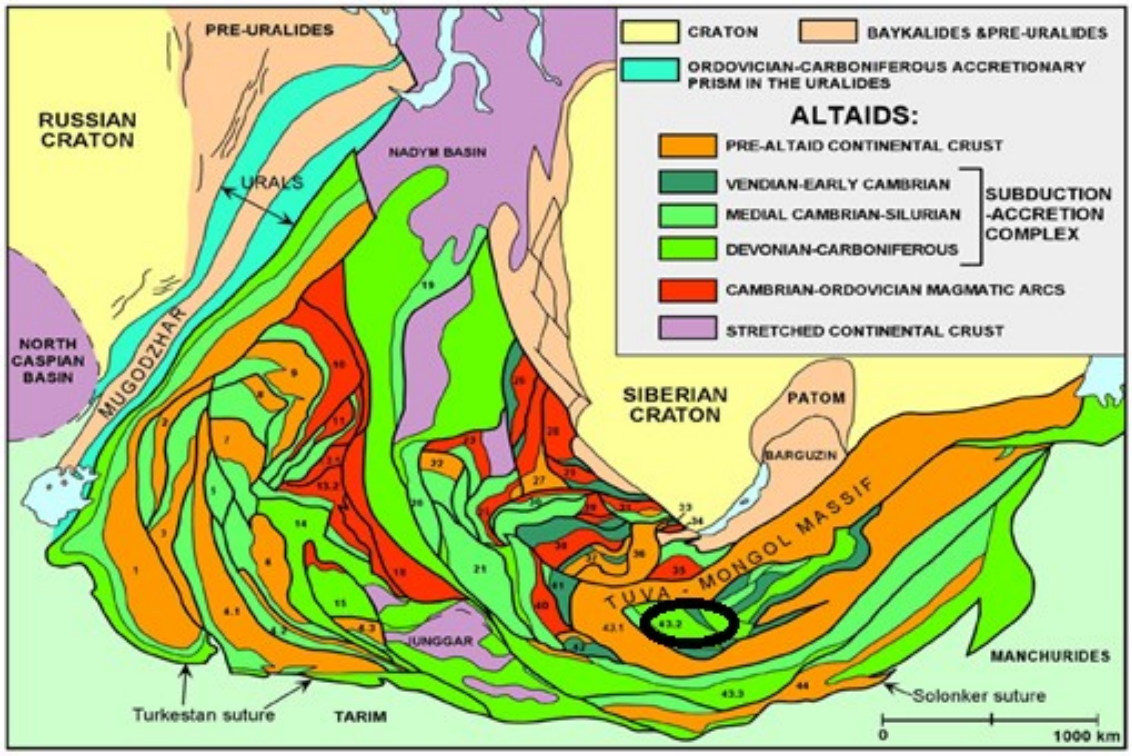

FIGURE 8. A generalized tectonic map of the COAB including the surrounding units. Note the location of the Tuva Mongol Massif, which surrounds the Hangay-Hentey Basin, (black circle). Image modified from (Şengör and Natal'in, 1996).

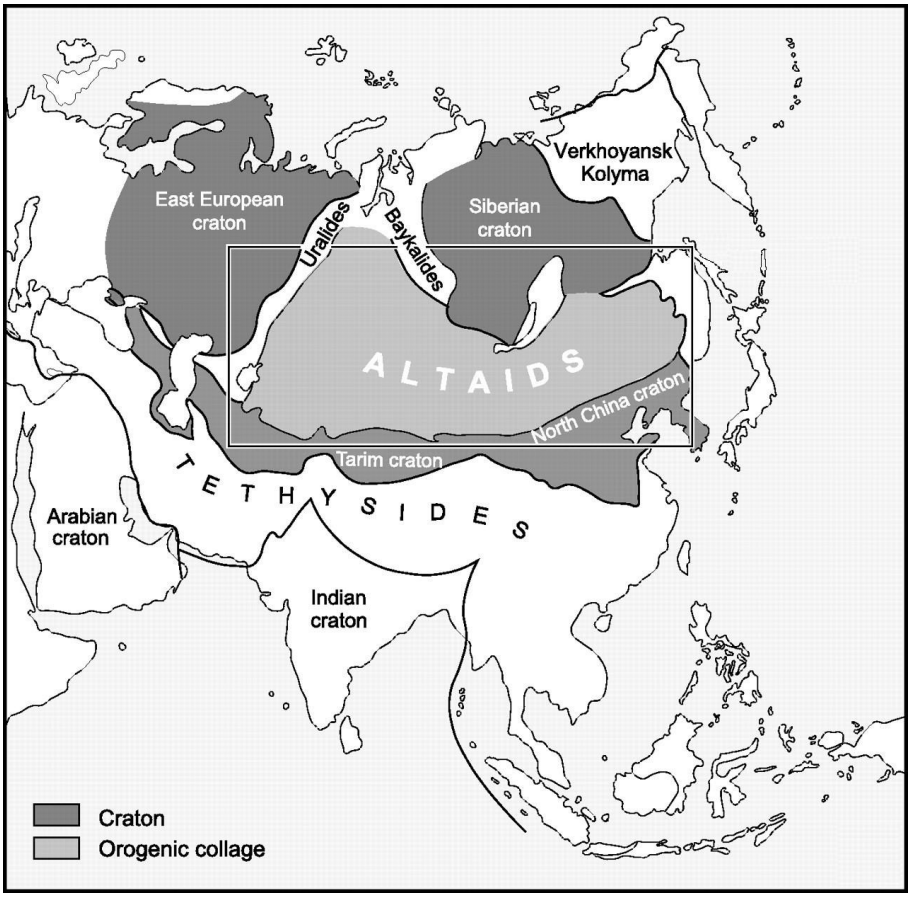

FIGURE 9. A more generalized map of the Altaids, also known as the CAOB that includes the surrounding cratons. The CAOB is outlined by a box. Image modified from (Şengör and Natal'in, 1996).

been adjacent to, and dipping towards, the Tuva Mongol Massif (Figure 10). Because the subduction zone dipped towards the Tuva Mongol Massif it then led to oroclinal rotation causing the closure of the Mongol Okhotsk Ocean forming the Hangay Hentey basin between the Devonian to Jurassic periods (Şengör and Natal'in, 1996).

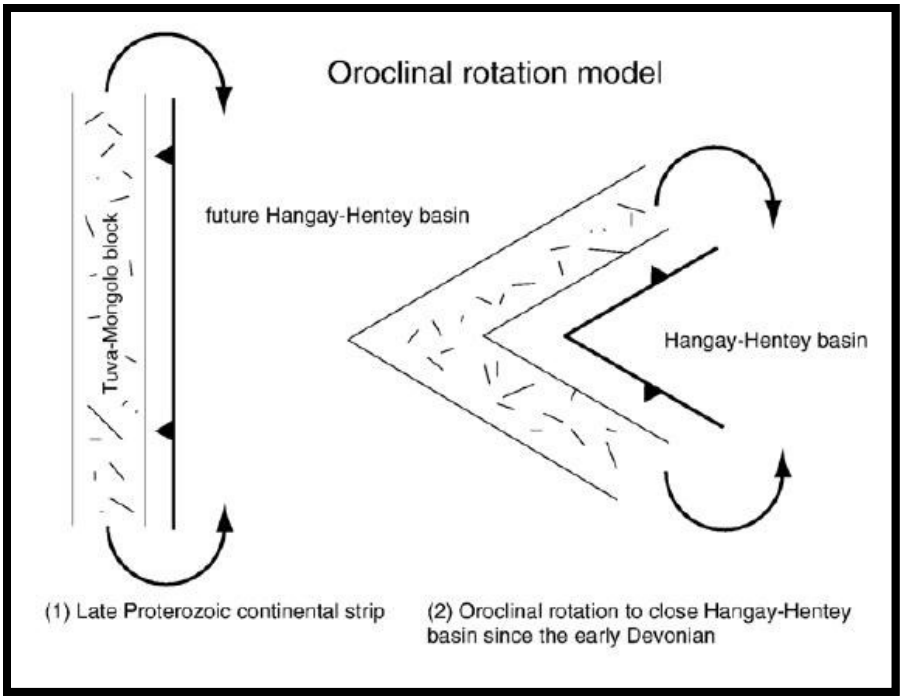

FIGURE 10. The Tuva Mongol Massif oroclinal rotation model. The massif surrounds the Hangay-Hentey basin. Image modified from (Şengör et al., 1993).

Scenario Two: Multiple Subduction Zones

The most accepted model for the formation of the CAOB describes the collision of multiple subduction zones and accretion of island arcs and microcontinents with the Siberia and China cratons (Badarch et al., 2002; Windley et al., 2007; Xiao et al., 2003; Xiao et al., 2004). Figure 11 shows a reconstruction of these collisions at 700 Ma and 550 Ma (Kuzmichev et al., 2005).

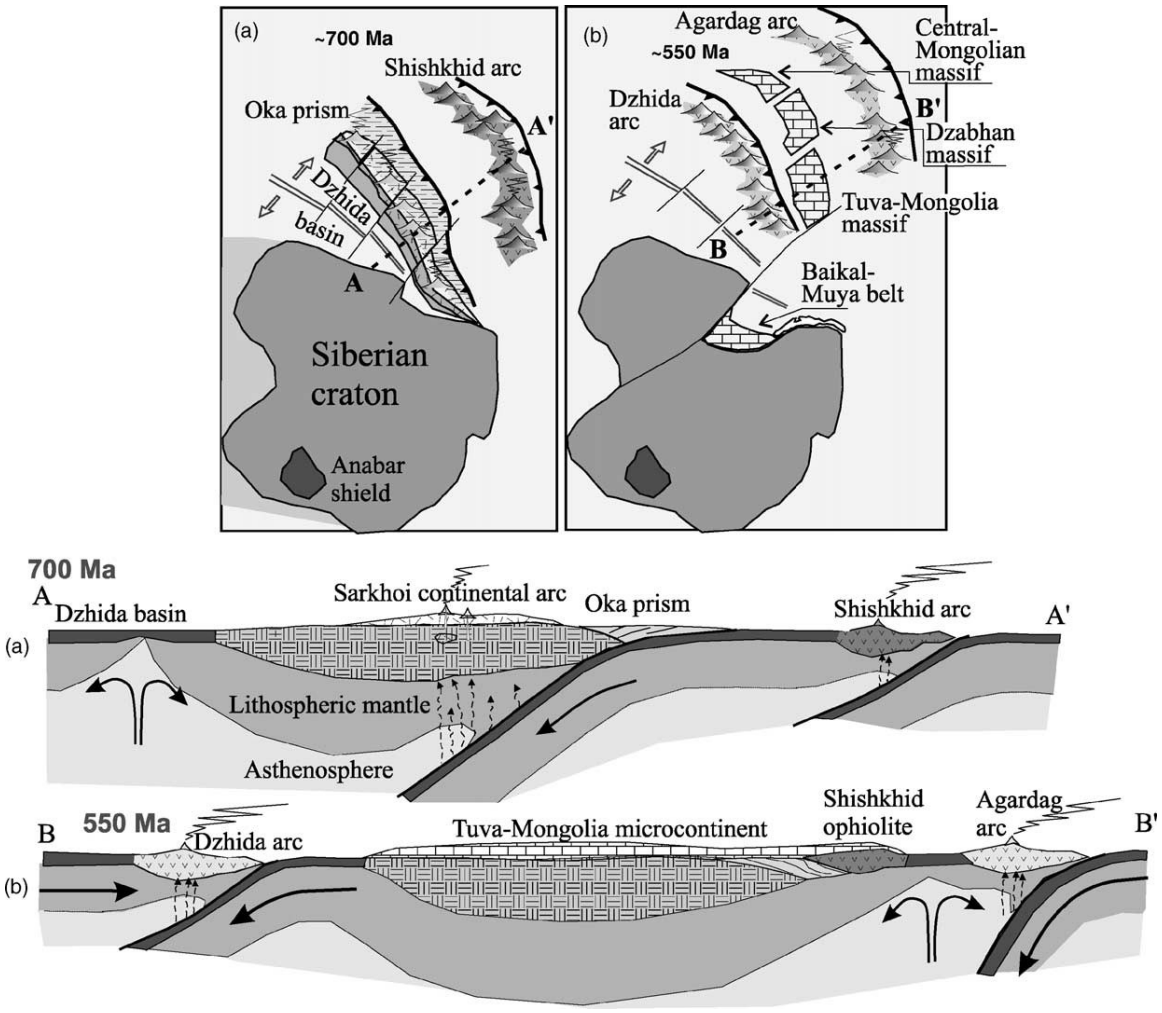

FIGURE 11. Model showing the evolution of the Siberian craton, island arcs, and microcontinents. A) Reconstruction around 700 Ma. B) Reconstruction around 550 Ma. Image modified from (Kuzmichev et al., 2005).

Figure 12 is a simplified tectonostratigraphic map of Mongolia which displays multiple subduction zones and the main lithologic units to the north and south of the Main Mongolian Lineament. Note the cross section line from A to B. This cross section will be represented in Figure 13, which shows the tectonic development of the Main Mongolian Lineament according to the multiple subduction zone model.

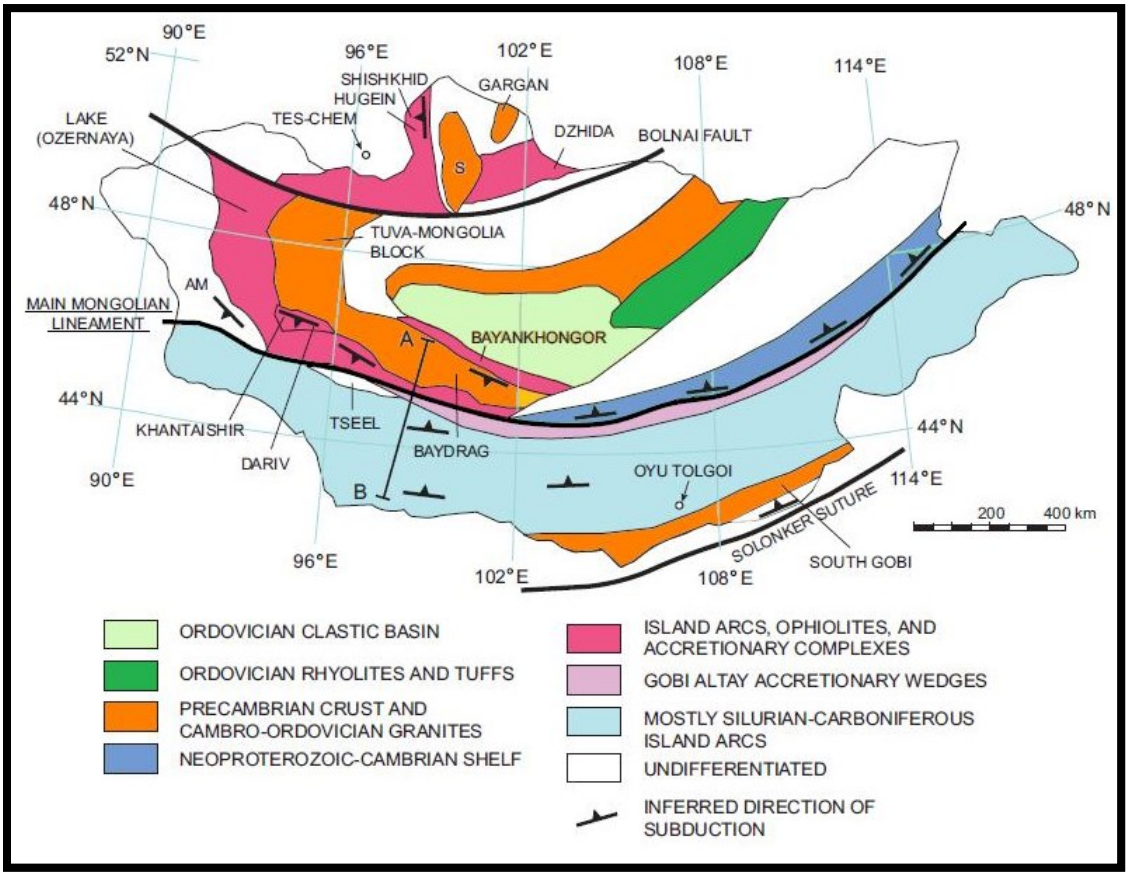

FIGURE 12. This map shows the major units to the north and south of the Main Mongolian Lineament. Image modified from (Windley et al., 2007).

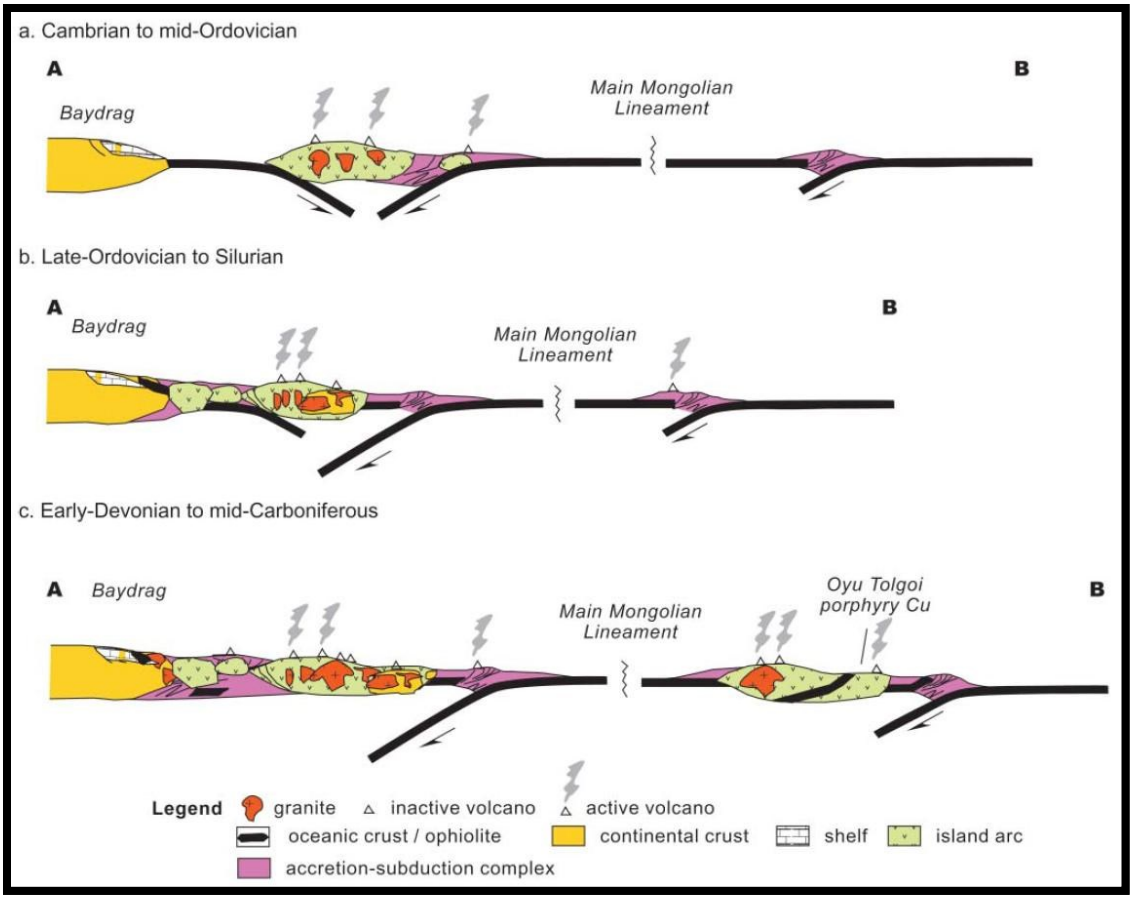

FIGURE 13. Cross sections from Figure 12, show the tectonic evolution from the Cambrian to Carboniferous periods. Image modified from (Enkin et al., 1992).

Collision of multiple island arcs and cratons eventually closed the Mongol-Okhotsk (M-O) Ocean (e.g., Delvaux et al., 1995; Zorin, 1999; Yin et al., 2005; Li, 2006; Kelty et al., 2008). Figures 14, 15, and 16 show reconstructions of the area from the Lower Jurassic to present day (Enkin et al., 1992). Note the position of the M-O Ocean and its closure over time. This closure formed the CAOB.

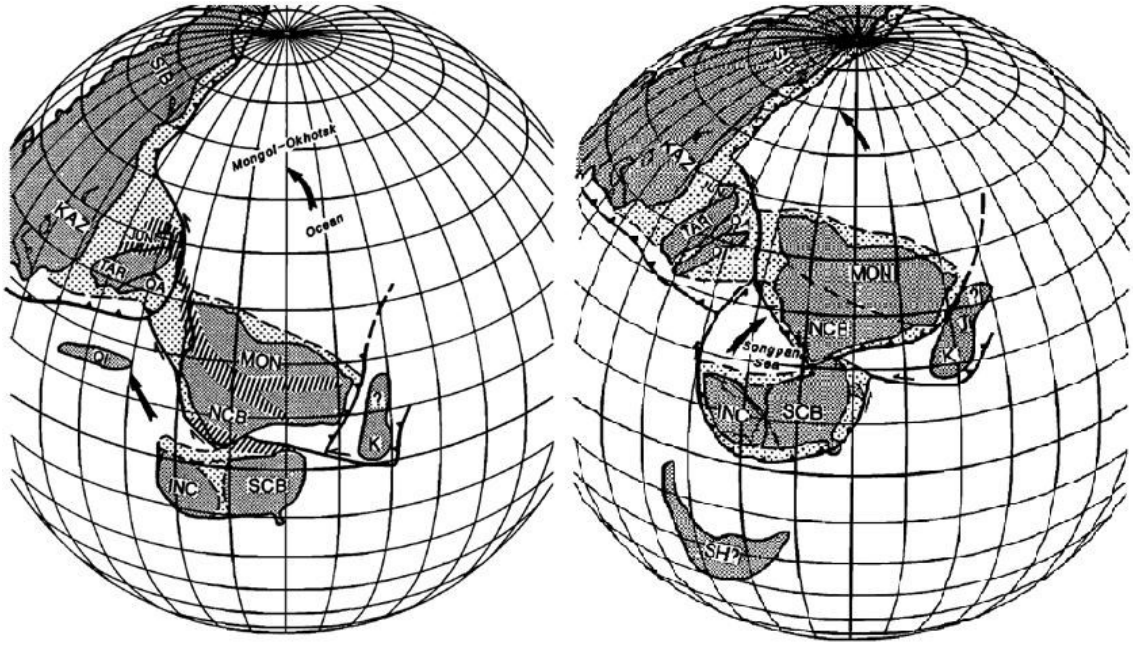

FIGURE 14. The left globe is the reconstruction during the Upper Permian (245-260 Ma). The right globe is the reconstruction of the Middle and Upper Triassic (205-240 Ma). Note the M-O Ocean north of the Mongolian craton. Image modified from (Enkin et al., 1992).

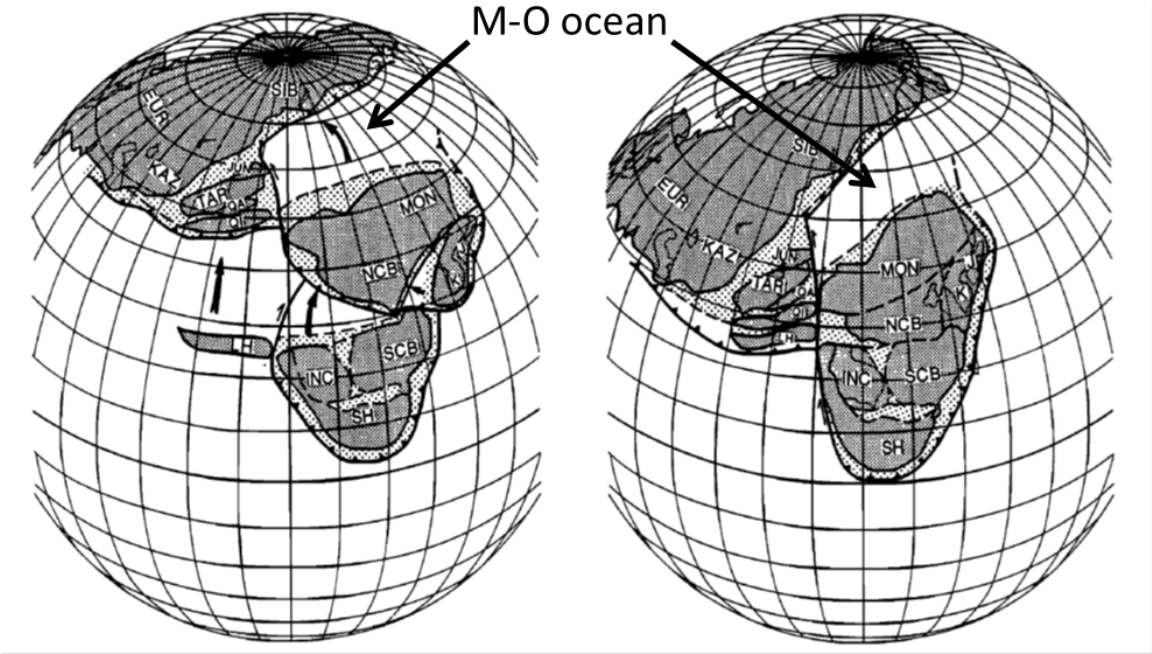

FIGURE 15. The globe to the left is the reconstruction during the Lower Jurassic (180-205 Ma); the globe to the right is the reconstruction during the Upper Jurassic. Note the M-O Ocean and its closure. Image modified from (Enkin et al., 1992).

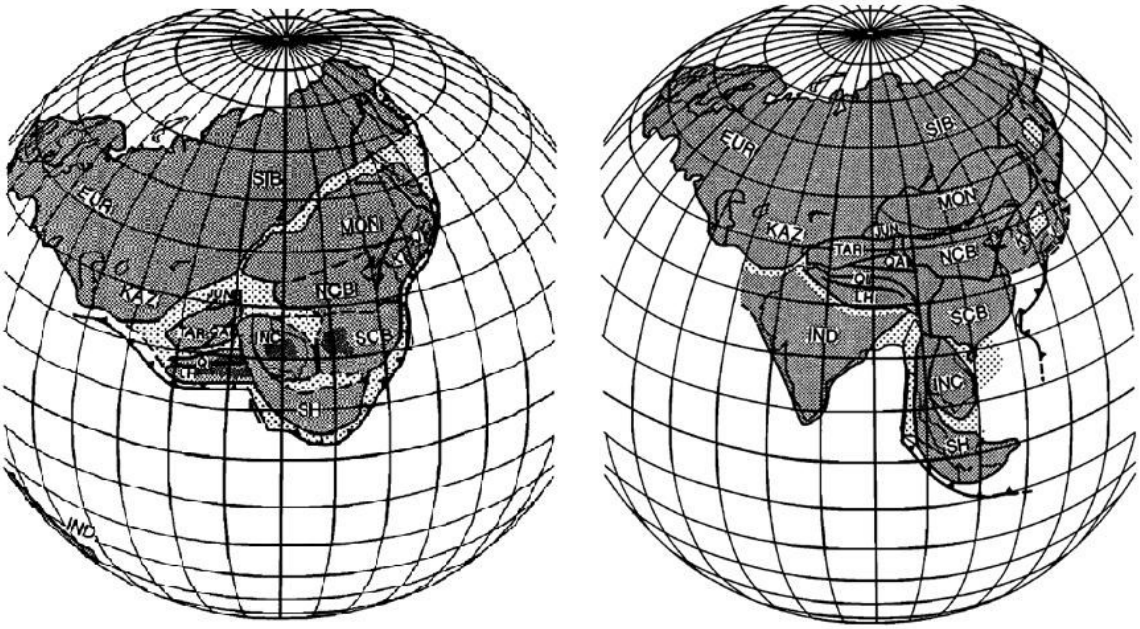

FIGURE 16. The left globe shows the reconstruction during the Lower Cretaceous (95 – 135 Ma). Note that the M-O Ocean is closed. The right globe shows present day configuration. Image modified from (Enkin et al., 1992).

Hangay-Hentey Basin Formation

The field area is located within the Hangay-Hentey basin which also has a controversial past. Zorin et al. (1993) describe the Hangay-Hentey basin as a former embayment between the Siberian craton and the Tuva-Mongol massif. The remains of the Tuva-Mongol massif collided with the Siberian craton in the late Proterozoic leading to the closure of the embayment and creation of the Hangay-Hentey basin. This model requires 90 degrees of rotation to form Tuva-Mongol massif and the Siberian craton in order for the basin to close. In this model the Hangay-Hentey basin closed by southward subduction along the southern side of the basin (Kelty et al., 2008; Figure 17)

Badarch et al. (2002) propose that the Hangay-Hentey basin formed in a back-arc setting. The basin formed as a continental strip (the Tuva-Mongolo block) rifted from the

Siberian craton, which formed a sea that was bounded by continuous continental crust on the northern and southern edges. This model has both north-dipping and south-dipping subduction zones on the southern arm of the Tuva-Mongol massif. The southern subduction had to occur before the northern subduction in order to generate a back-arc basin (Figure 18). This model requires less than 40 degrees of rotation between the Siberian craton and the southern arm of the Tuva-Mongol massif.

Terranes of Mongolia

Mongolia is composed of numerous terranes and super terranes that extend past Mongolia's borders (Badarch et al., 2002; Tomurtogoo, 2002). The terrane map referenced for this study was published in 2002 by the Institute of Geology and Mineral Resources. The study area falls within three different terranes. These terranes include the Harharin turbidite terrane, the Testserleg turbidite terrane, and the Ulaanbaatar turbidite terrane (Figure 19). The rocks within these terranes are mostly Devonian and are cut but younger granites. The Harhorin turbidite terrane includes quartzite, red chert, quartzite schist, sandy schist, and meta-sandstone formations (Tomurtogoo, 2002). The Tsetserleg turbidite terrane includes siliceous-terrigenous, sandstone and siltstone, greywacke, and is stitched to other terranes by granodiorite or granite (Tomurtogoo, 2002). The Ulaanbaatar turbidite terrane includes volcanic schist, chert, terrigenous mollasse, and granodiorite-granite intrusions (Tomurtogoo, 2002). These terranes are referenced to aid in the understanding of the geology the field area.

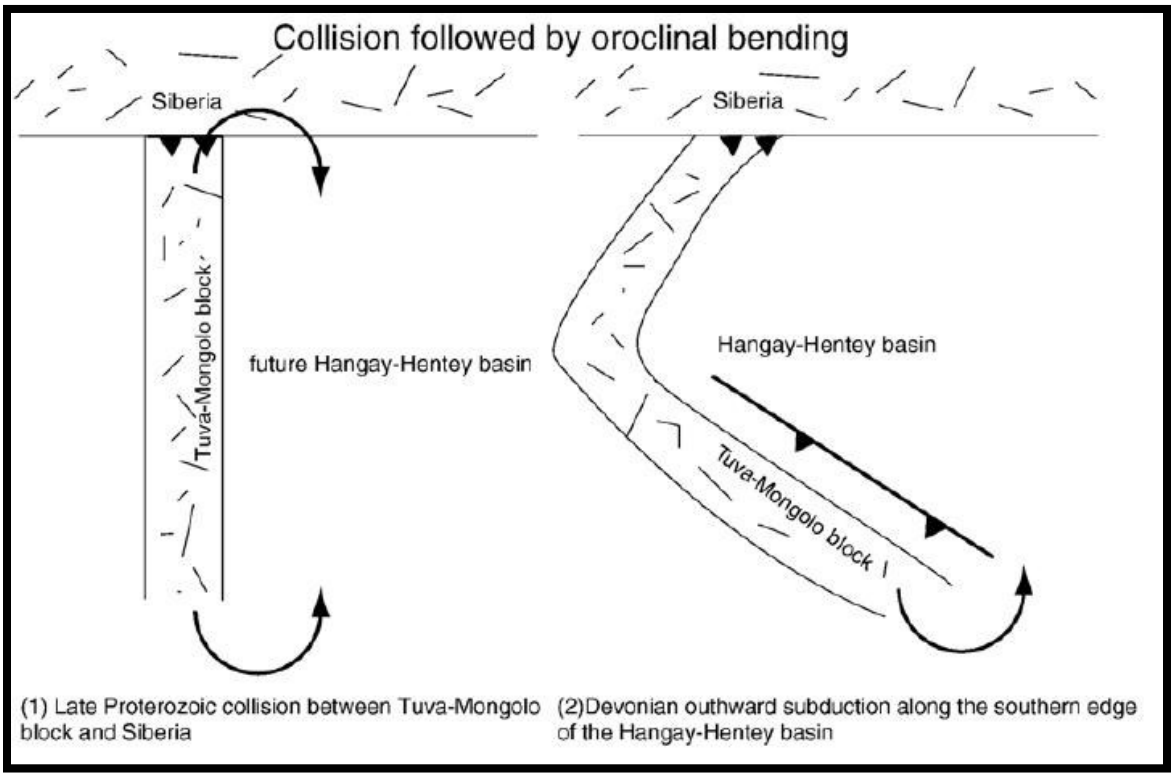

FIGURE 17. Formation of the Hangay-Hentney basin began with the Tuva-Mongol Massif colliding with the Siberia craton but was later oroclinally rotated closing the Hangay-Hentey basin. Image modified from (Zorin et al., 1993).

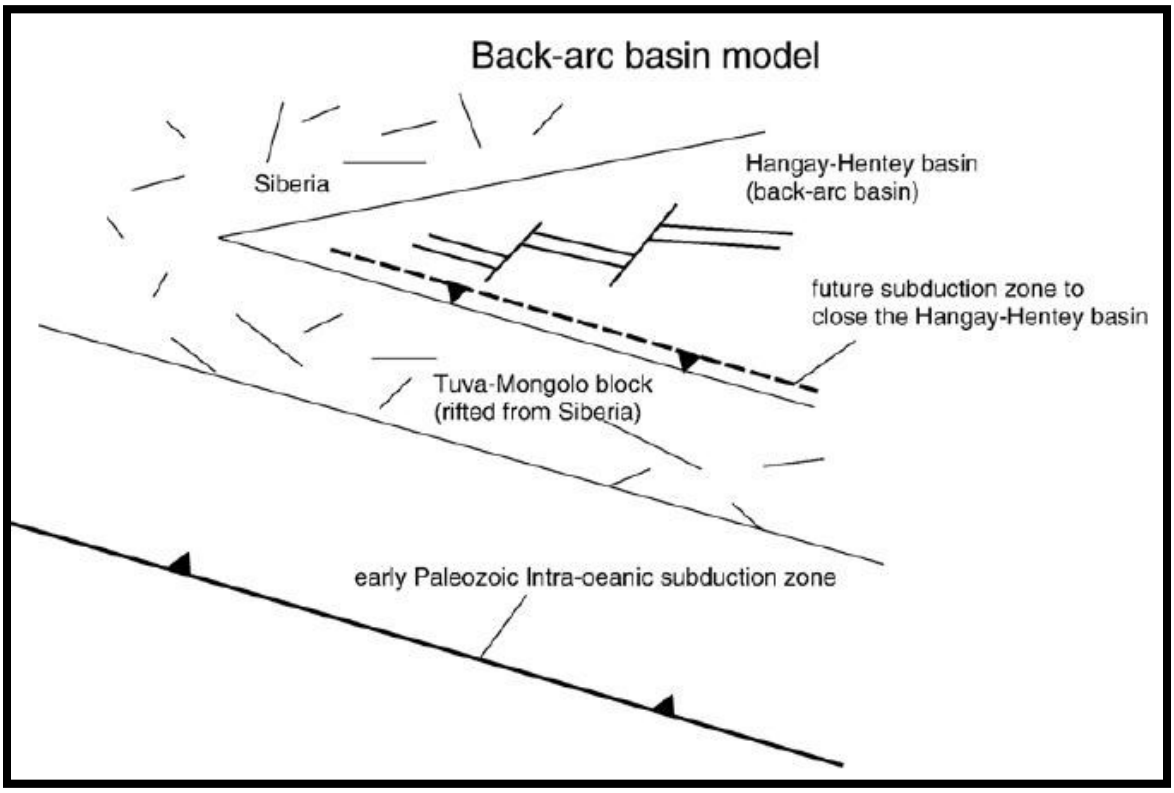

FIGURE 18. Back-arc basin model used to show the formation of the Hangay-Hentey basin. Image modified from (Badarch et al., 2002).

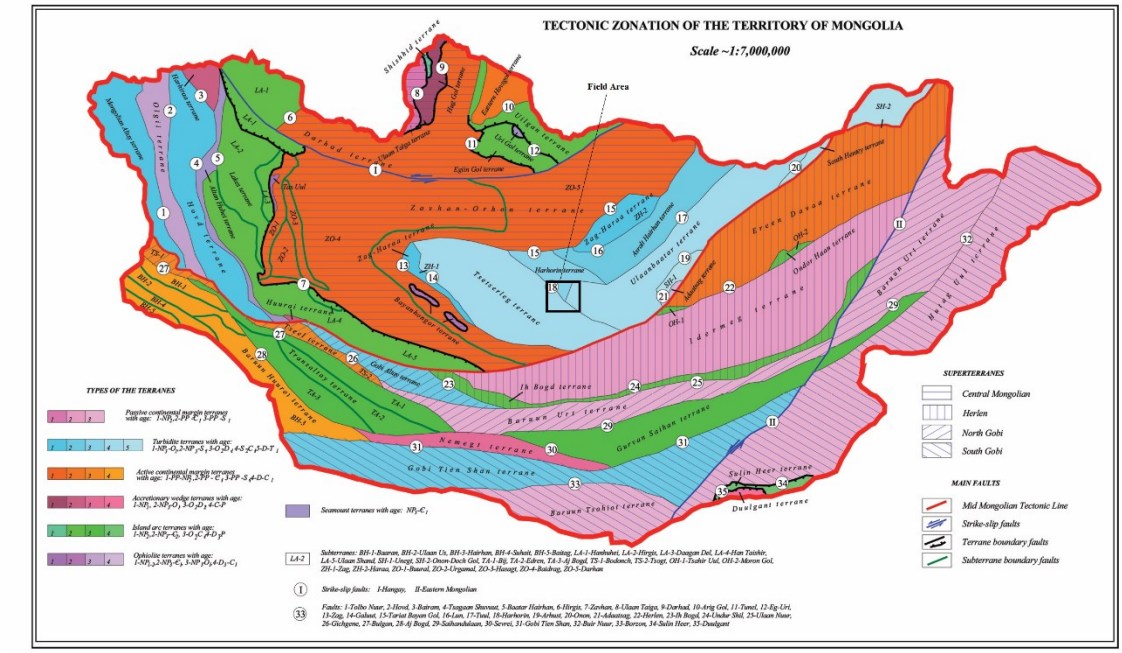

FIGURE 19. Terrane map of Mongolia. Field area denoted by a black square. (Modified from Institute of Geology and Mineral Resources, 2002).

Faults and Active Tectonics

The active tectonics of central Mongolia are caused by the collision of India and Eurasia (e.g., Tapponier and Molnar, 1979). Mongolia has experienced considerable amounts of seismic activity. Table 1 shows a list of earthquakes in Mongolia with a magnitude greater than 8.0 on the Richter scale that occurred during the 1900s. Before 1994 the earthquakes were recorded by analog stations and measured in K energy (ML) a scale used in Russian scientific community, this data was later recalculated into the Richter magnitude scale (Ankhtsetseg et al., 2007). The large Mongolian earthquakes include the Tsetserleg and the Bulnay earthquakes in 1905 and the Gobi-Altay in 1957, which occurred approximately 460 km, 550 km and 330 km from the study area,

respectively. Figure 20 illustrates a seismicity map of Mongolia that shows the magnitude and distribution of earthquakes recorded between the years 1900 to 2000.

TABLE 1. Shallow Earthquakes in Mongolia (Kurushin et al., 1997)

Year	Name	Place	Latitude (°N)	Longitude (°E)	Magnitude (M)
1905	Bulnay	Northern Mongolia	49.2	96	8.7
1905	Tsetserleg	Northern Mongolia	49.5	97	8.4
1957	Gobi-Altay	Mongolia	45.31	99.21	8.3

GPS measurements show the central Mongolia region has been moving east with respect to Siberia while Eurasia remains stable and India has moved northward Walker et al.(2008). This movement places the Hangay Mountains, which are to the west of the field area, between two east-west, left- lateral fault systems: the Bulnay fault system to the north and the Gobi-Altai fault system to the south (Walker et al., 2008). The Hangay Mountains are considered a rigid block in the India-Eurasia collision because of the lack of seismicity (Walker et al., 2008). However, there is evidence of active faults in this region. For instance, normal faults with evidence of Quaternary movement have been mapped in the Hangay Mountains (Tapponnier and Molnar, 1979; Baljinnyam et al. 1993; Cunningham, 2001; Walker et al., 2008). Strike-slip faults are also found in the Hangay area and accommodate the left-lateral shear between Siberia and China (Walker et al., 2008). The presence of active faulting within the Hangay Mountains could indicate that there is active faulting in the basin as well. Figure 21 shows a map of the field area and its proximity to the Hangay Mountains.

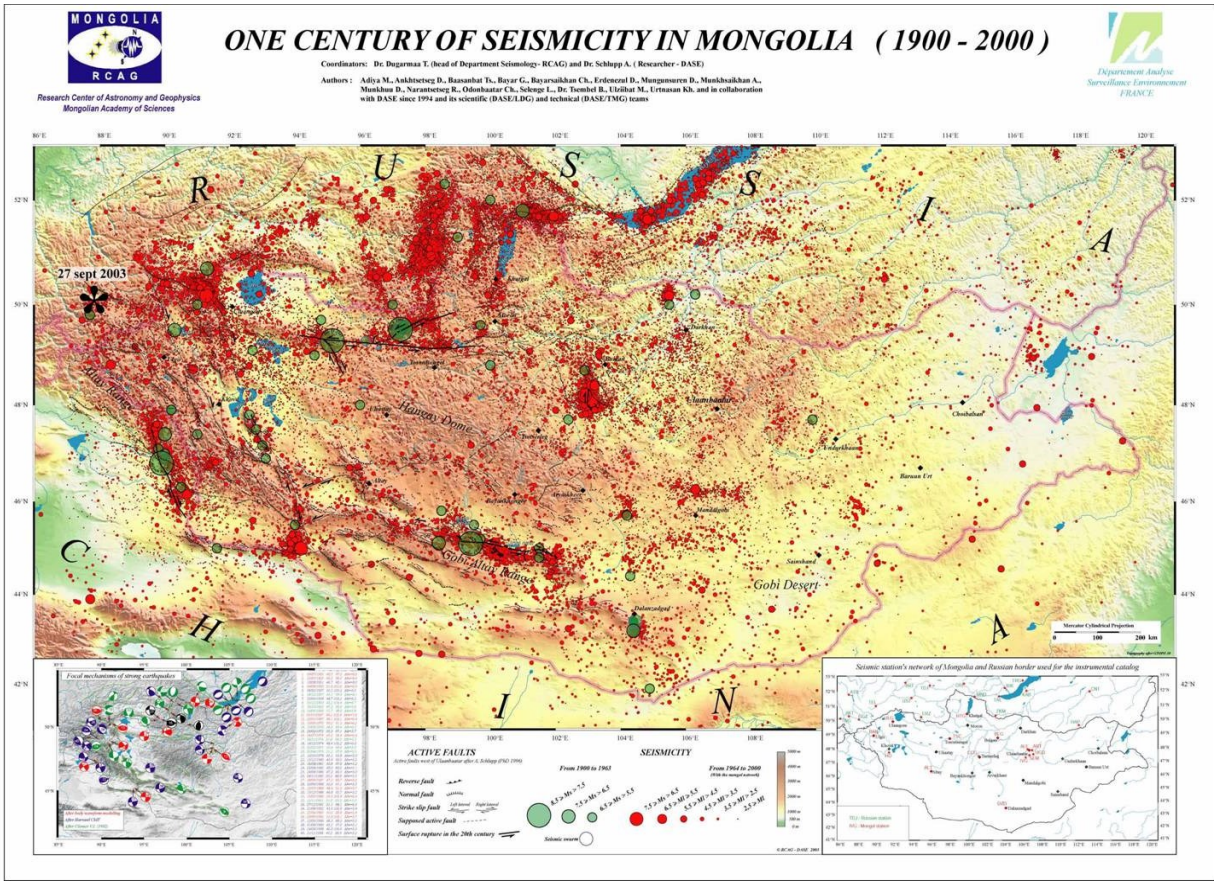

FIGURE 20. Seismicity map of Mongolia from 1900 to 2000. The green circles are earthquakes that occurred from the year 1900 to 1963 and the red circles are earthquakes that occurred from the year 1964 to 2000. The circle size represents the earthquake magnitude. Image modified form Dugarmaa et al. (2003).

In the Hangay Mountains, Walker et al. (2008) identified and described a set of faults that include the Songino-Margats, the Hag Nuur, the Uliastay, and the South Hangay fault systems. These faults are located in the southern and the eastern sections of the Hangay Mountains and are east-west, left-lateral stike-slip faults. They show evidence of late Quaternary activity from surface expression in the form of aligned sequences of sag-ponds and pressure-ridges (Walker et al., 2008). There is also evidence

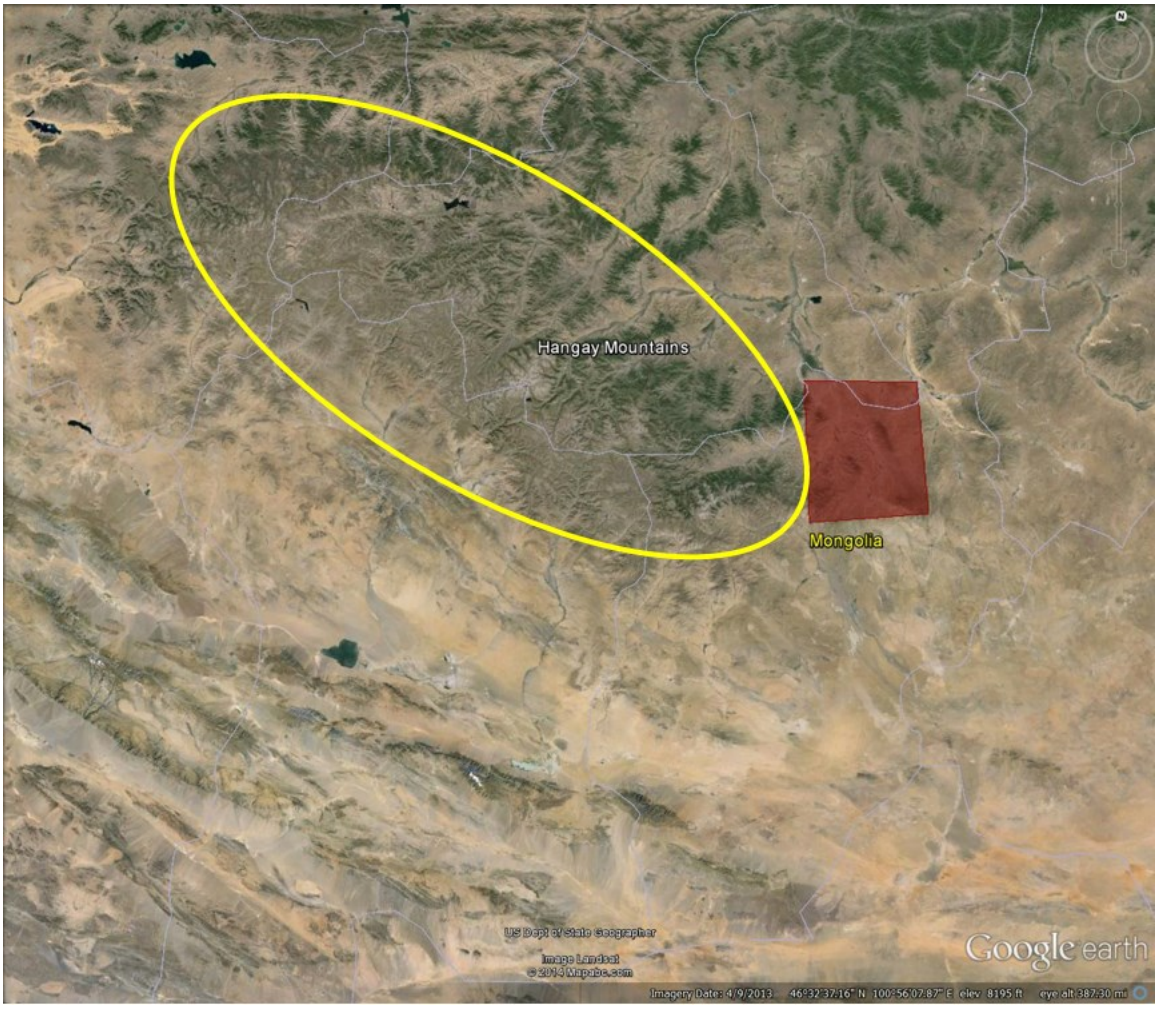

FIGURE 21. A satellite image of the field area, outlined in red, in relation to the Hangay Mountains, outlined in yellow.

of bedrock being displaced about 3 km along both the South Hangay fault systems and the Songino-Margats. These faults are over 250 km west of the field area.

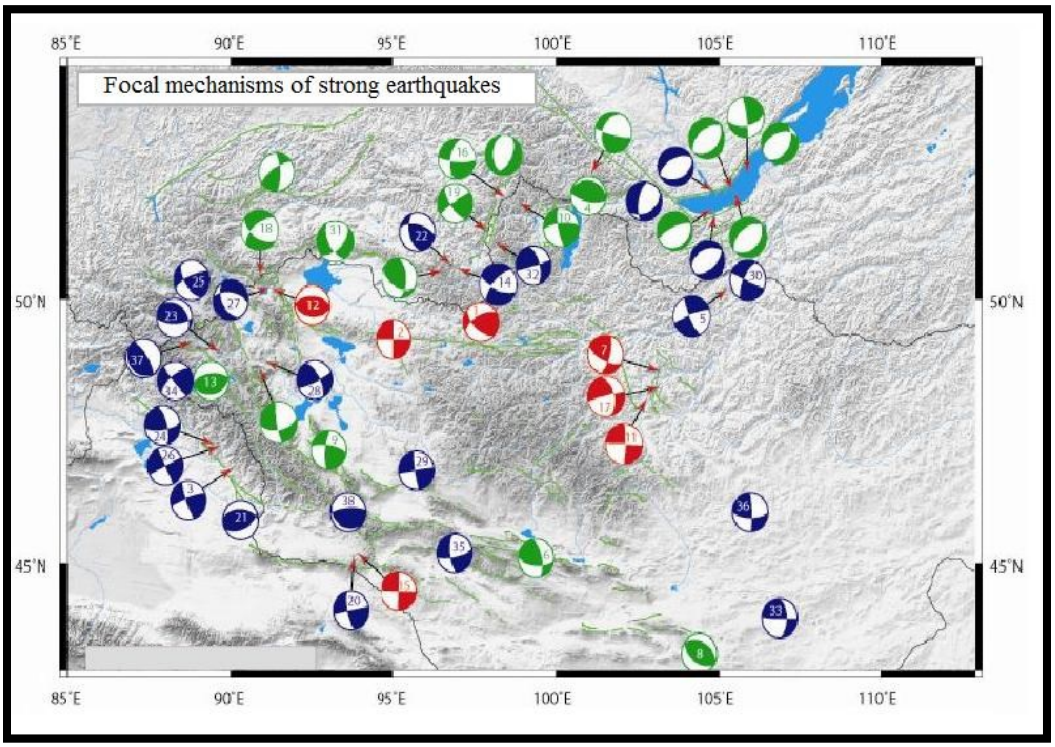

FIGURE 22. Focal mechanisms of the major earthquakes in Mongolia. The different colors represent different models. The focal mechanisms are represented by beach ball diagrams, compression (colored section) and tension (the white section). Strike slip faults are represented with an "X" with both color and white sections. Normal faults are represented with white in the middle. Reverse faults are represented by colored section in the middle. Image modified from Dugarmaa et al. (2003).

The focal mechanisms in Figure 22 show that the north-south striking faults tend to be right-lateral strike-slip faults and the east-west striking faults tend to be left-lateral strike-slip faults.

Ankhtsetseg et al.(2007) constructed a seismic hazard and risk map of Mongolia. They determined the occurrence and distribution of earthquakes and have related the seismicity to geologic structures and tectonic processes. Ankhtsetseg et al. (2007) noted that the current seismic station coverage is lacking in eastern Mongolia. Mongolia has a lot of seismic coverage to the west, but not to the east. Due to the instrumentation they use, earthquakes with a magnitude less than 3.5, which constitute most earthquakes, cannot be detected (Ankhtsetseg et al., 2007).

Geologic Maps

The debate about Mongolia's geologic history is partially due to inconsistent, old data that are ambiguous and unsupported (Lamb and Badarch, 1997). Also, there is a lack of research due to its remote location. Cocks and Torsvik (2005) describe the geologic maps as oversimplified or inaccurate and the literature as having ambiguous geologic terminologies and terrane names. Additionally, old Russian literature used geosynclinal models, which have been replaced by the plate tectonic theory, to describe the formation of Mongolia (Delvaux et al., 1995).

According to the Institute of Geology and Mineral Resources, Mongolia has been geologically studied for more than 100 years. The first geologic map was published in 1957 at a scale of 1:2,500,000 (general editor: Academician V.A. Obuchev). In 1997 and 2002 newer geological maps were produced by the Institute of Geology and Mineral Resources of the Mongolian Academy of Sciences. There are 2 maps, one is titled "Geological Map of Mongolia at a scale of 1:1,000,000" (e.g., Figure 23). The components of the geologic map include major rock types and their distributions,

geological age and relationships and tectonic faults. The second map is a tectonic map of Mongolia and it was published in 1999-2002 titled “The Tectonic Map of Mongolia at a scale of 1:1,000,000” (e.g., Figure 24).

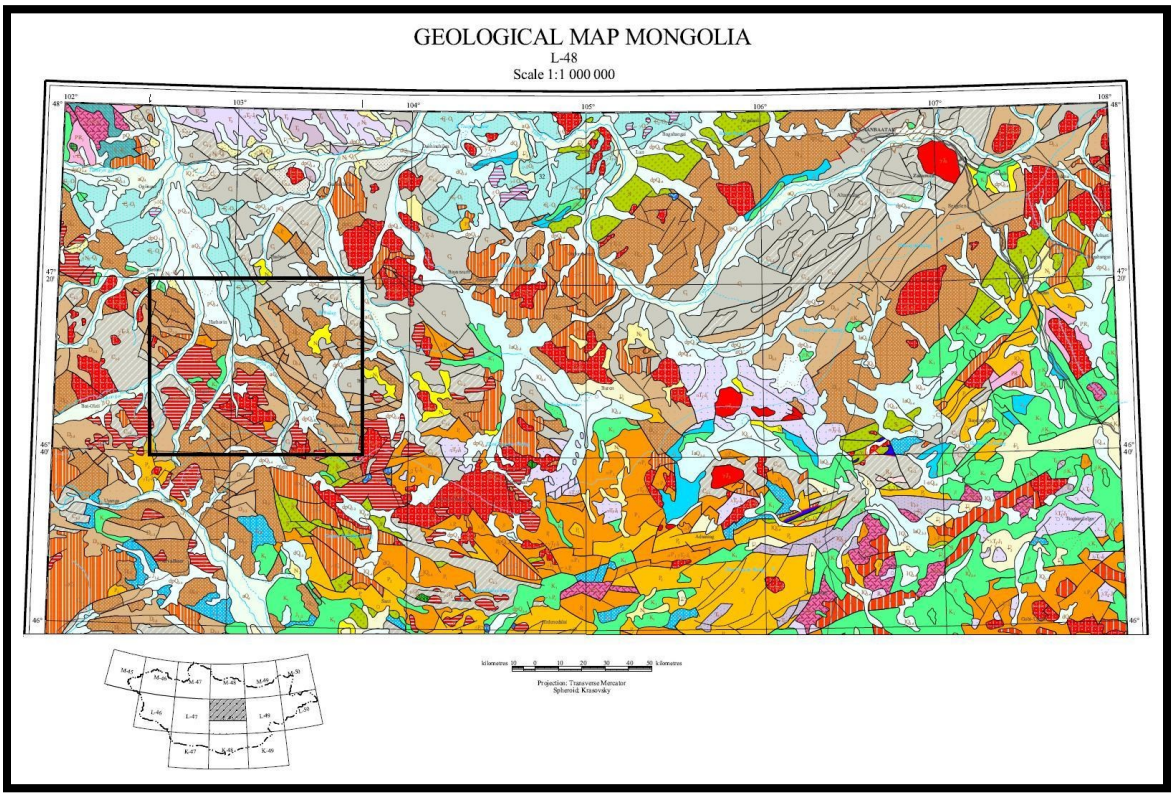

FIGURE 23. Geological Map of Mongolia from Institute of Geology and Mineral Resources of Mongolia (1998). The black square marks the field area.

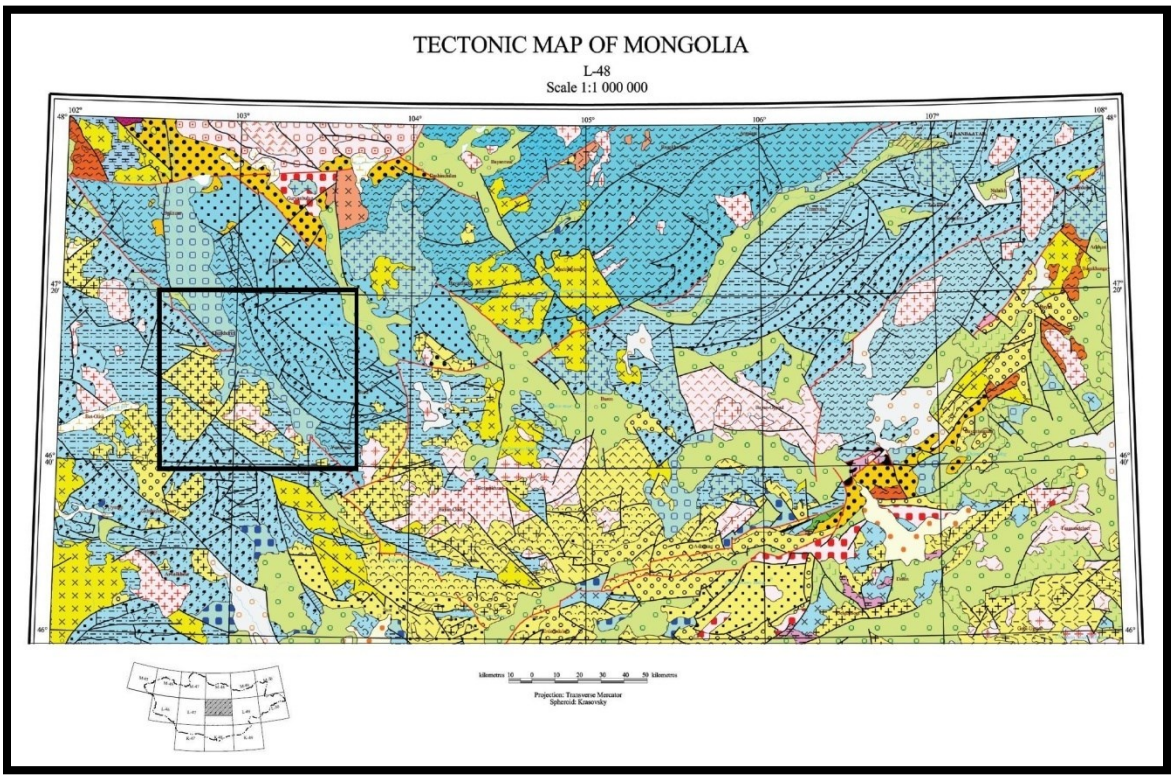

FIGURE 24. Tectonic Map of Mongolia. The black square outlines the field area (modified from Institute of Geology and Mineral Resources, 2002).

CHAPTER 3

METHODS

Location and Accessibility of Study Area

The faults and outcrops that were assessed are located approximately 320 kilometers (km) southwest of Ulaanbaatar (UB), Mongolia (Figure 25), which is located at 47°54'N, 106°52'E. Tactical Pilotage Charts along with satellite images were used to navigate to the field area. The field area was reached from UB by a combination of discontinuous paved highways, dirt roads, and off-roading. The field area was traversed using a four-wheel drive vehicle.

Field Studies

Field work was conducted June through July, 2010. The location of each outcrop was determined with a hand-held Garmin GPS eTrex Legend® receiver, which has an accuracy of up to 15 meters. The GPS was set to use the world geodetic system (WGS) 84 datum, and displayed location in latitude and longitude and recorded the information in DMS (Degrees/Minutes/Seconds). A Brunton® compass, with a magnetic declination of zero degrees, was used to measure orientations of faults, bedding, lineations, and foliations. The measured kinematic data were then analyzed using the program Stereonet 8 (Allmendinger, 2013). The lithology of each outcrop was described, and rock samples were brought back to the United States. Also, a series of photographs were taken of

FIGURE 25. The field area is noted as a red square that is within two provinces the Arkhanga and the Övörhangay. The field area is also located south-west of Ulaanbaatar (Google Earth).

landscapes, faults, and rock outcrops. The use of satellite imagery and documented latitude and longitude was used to record field data. Field data was plotted on the imagery and recorded in a field notebook.

ENVI ("Environment for Visualizing Images") is a software application used to process and analyze geospatial imagery. Landsat 7 satellite image data were obtained from the USGS, and processed in ENVI to create maps in both true and false color. The program processes the electromagnetic wavelengths and places them into bands that represent three colors in the visual spectrum: Red (3), Green (2), Blue (1). A true color map would be represented as 3, 2, 1. False color images allow a viewer to perceive

different wavelengths from the electromagnetic spectrum, outside of the range of the visual spectrum, and the program displays it as red, green, and blue. This is valuable because it can accentuate features that may not be otherwise discernible.

False color images for this thesis were created by using the 7, 4, and 2 bands. Mid-infrared is band 7, near- infrared is band 4, and green is band 2. In a 7, 4, 2 false color image vegetation will appear bright green, pink areas describe barren soil, and oranges and browns represent sparsely vegetated areas (Jensen, 2007). This false color image also highlights differences in rock types and is useful in identifying contacts. Table 2 shows the different wavelengths captured in Landsat 7 images and their associated bands.

TABLE 2. System Characteristics of the Enhanced Thematic Mapper Plus (ETM+) (Jensen, 2007)

Enhanced Thematic Mapper plus		
ETM+		
Landsat	Wavelength	Resolution
7	(Micrometers)	(Meters)
Band 1	0.450-0.515 (blue)	30
Band 2	0.525-0.605 (green)	30
Band 3	0.630-0.690 (red)	30
Band 4	0.750-0.900 (near IR)	30
Band 5	1.55-1.75 (mid IR)	30
Band 6	10.40-12.50 (thermal IR)	60
Band 7	2.08-2.35 (mid wave IR)	30
Band 8	0.52-0.90 (panchromatic)	15

Note: IR stands for infrared

Esri's ArcGIS® is a geographic information system (GIS) that is used for working with maps, creating maps, and organizing geographic information. ArcGIS was used to create geologic maps and to manage a geographic database of field data.

Map Creation

For this project, both the Institute of Geology and Mineral Resources Geologic Map of Mongolia (1998, Figure 23) and the Tectonic Map of Mongolia (2002, Figure 24) were used as a reference in the process of creating a geologic map at a scale 1:100,000. These maps were refined by incorporating observations in the field that could be correlated using false and true color satellite imagery. This resulted in a geologic map covering approximately 8,072 km^2 and at a scale of 1:100,000 (Plate 1).

Geomorphic Indices

Geomorphic indices are used to quantify different aspects of landforms such as, the asymmetry of a basin, or the gradient of a stream along its profile. These can aid in the determination of active faulting in an area, for instance, if two adjacent basins are highly asymmetric than it implies the presence of a fault. For this study three indices were used to identify if the Sangiin Dalai Nuur and Ereen Uul faults (Plate 1) are active: hypsometry, asymmetry of a mountain range, and stream length-gradient index. The process for evaluating these geomorphic indices was taken from Keller and Pinter (1998).

Hypsometry is a measurement of the area of land at different elevations. It can be broken down into the hypsometric curve and the hypsometric integral. The hypsometric curve is a graphical representation that shows the distribution of elevations over an area.

The values for this curve were derived from DEM data in ArcGIS. This graph is used to determine the maturity of the landscape. Variables that were retrieved or computed in ArcGIS include: H is equal to the maximum elevation minus the minimum elevation, h is equal to a given line of elevation, A is equal to the sum of the areas between each pair of adjacent contour lines, a is equal to the surface area of a basin above an elevation (h), h/H is equal to the relative height, and a/A is equal to the relative area.

The value of the relative area (a/A) of a basin varies from 1.0 to 0. When (a/A) is equal to 1 the relative height (h/H) is equal to 0. At the highest point of the basin, when (h/H) is equal to 1 the relative area (a/A) is 0. The elevations are plotted as functions of total area and total elevation allowing for the drainage basins of different sizes to be compared with each other. The hypsometric integral (H_i) was used to determine the shape of the hypsometric curve of a drainage basin and is defined as

$$H_i = (h_{mean} - h_{\min}) / (h_{\max} - h_{\min}) \qquad (1)$$

where h_{mean} is the average elevation, h_{max} is the maximum elevation, and h_{min} is the minimum elevation. High values of the integral indicate that the topography is high compared to the average, which is associated with smooth upland surfaces that are cut deeply by incised streams. Low to intermediate values of the integral are associated with drainage basins being more evenly cut by streams. This information leads to the determination of the age of the landscape as either youthful, mature, or old (Keller and Pinter, 1996). If the topography is young it is an indication that the area was recently uplifted.

The asymmetry of a mountain range was examined next to the Ereen Uul fault. This evaluation was done by comparing the size of the drainage basins on either side of the mountain range. If the drainage basins have close to equal area then the uplift along the mountain range is uniform. If the drainage basins on one side of the range are greater than the other side, it can be evidence that the mountain range is lifting asymmetrically.

The stream length gradient index (SL) is a measure of the relationship of rock resistance and topography and looks at the changes in slope over a given length of stream. It is used in this study to look for possible active faulting. The SL is equal to the $(\Delta H / \Delta L) * L$. The ΔH is the change in elevation of the reach. The ΔL is the length of the reach. L is the total channel length from the midpoint of the reach of interest up stream to the highest point on the channel.

The SL was calculated using a DEM in ArcGIS. For this study the following steps were followed to determine the SL for both the Ereen Uul fault and Sangiin Dalai Nuur fault. First, points were placed along the stream moving from the outflow up to the headwaters. Second, the elevation of each point was extracted from the DEM. Third, the coordinates of each point were used to determine their distance between each of these points. Forth, a stream profile for each stream of interest was plotted. Fifth, the above equation was used to calculate the SL index for a segment of the stream.

Because stream profiles adjust quickly to rock resistance during landscape evolution (Keller and Pinter, 1996), this method can be used to indicate recent faulting. Unusually high SL indices in soft rock may indicate active or recent tectonic activity. Abnormally

low values may also indicate faulting where strike slip faults have weakened rock within the fault zone (Keller and Pinter, 1996).

CHAPTER 4

RESULTS

Maps and Field Data

Data was collected at a total of 146 locations that expand across an area of 8,072 km^2. A satellite image with each of these field locations and the two faults studied is shown in Figure 26. In the area studied the elevation ranges from 1,182 meters above mean sea level (MSL) to 2,495 meters MSL. This data was used in conjunction with remote sensing to create a geologic map (Plate1). A geologic cross section was constructed crossing through the two faults studied (Plate 1). Going from southwest to northeast the cross section shows right lateral strike slip movement along the Sangiin Dalai Narr fault followed by intrusive rocks in the center, to more right lateral strike slip faults and ends with a normal fault, mapped as the Ereen Uul fault.

This study was focused on the construction of a geologic map at a scale of 1:100,000 and on the activity of faulting along two faults in the study area. Within the study area there are three terrains and twelve different units as described by (Tomurtogoo, 2002). The three terranes include Harhorin turbidite terrane, Testserleg turbidite terrane, and the Ulaanbaatar turbidite terrane. These terranes which are described in the Regional Geology section are mostly Devonian in age and are cut by intrusive granites. As noted in the methods section, the contacts of each of the twelve

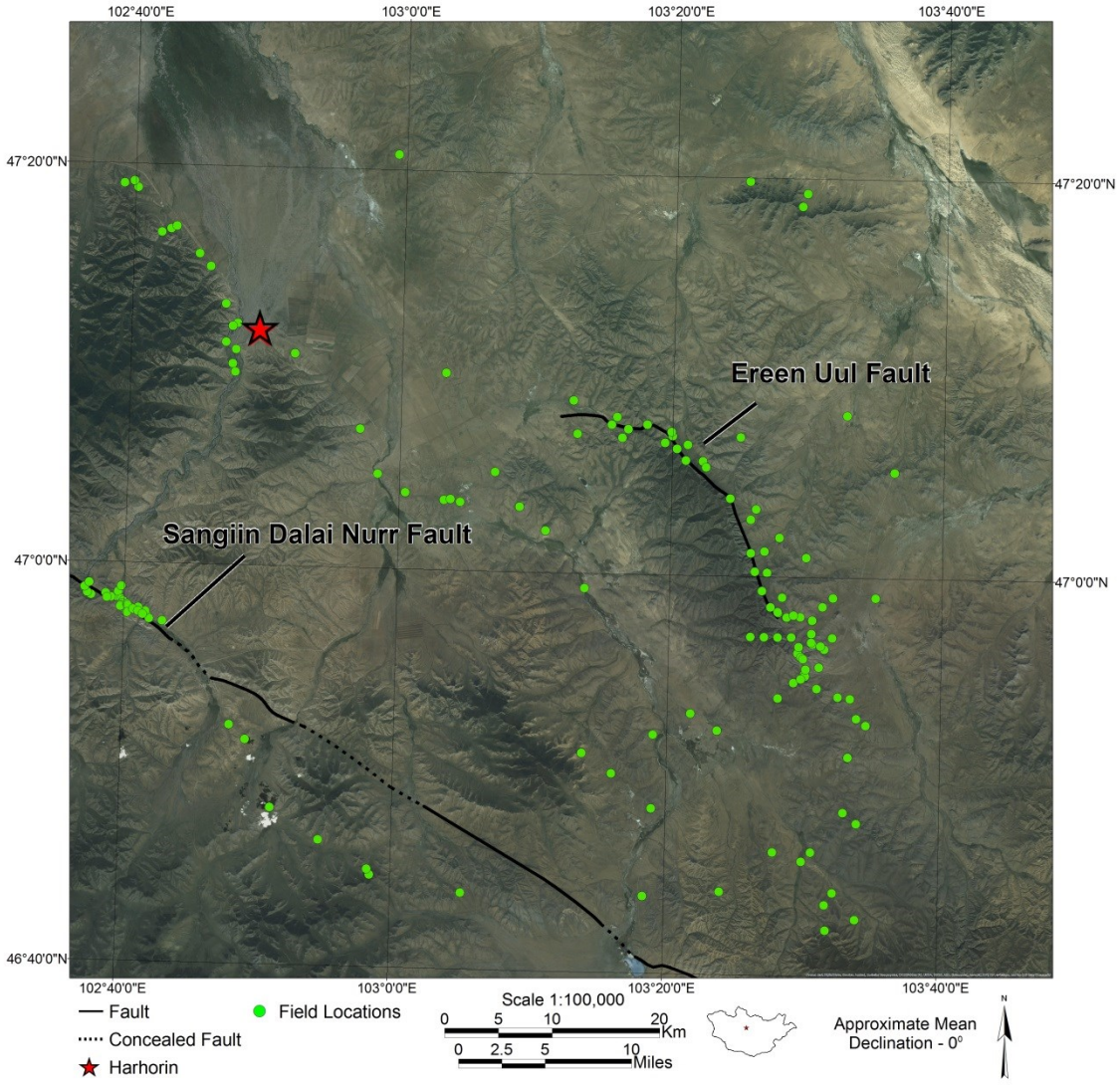

FIGURE 26. Study area and field locations.

units have been updated and the lithologic description has been described for the field area. The rock names and ages are that were used for this study are from the Institute of Geology and Mineral Resources, 2002. Plate 1 shows a map of the units

including the age of each unit. Each of the rock types is described in chronological order below.

The Basalt is located in the northwest (plate 1). The basalt is a dark gray (figure 27).

FIGURE 27. Rock outcrop of basalt.

Granites (Triassic to Jurassic?) are located in the middle southern section of the map (Plate 1, Figure 28).

FIGURE 28. Picture of the granite (Triassic to Jurassic?).

Granites (Permian?) are located from the southeast and west of the map (Plate 1, Figure 29).

Oligomictic terrigenous rocks are located on the east and north east side of the map (Plate 1). This rock is fine to medium grained sandstone with some interbedded shales. The rocks has a small degree of metamorphism and weather orange red and have a dark grey coating while fresh surfaces are gray green to orange brown (Figure 30).

FIGURE 29. Picture of the granite (Permian?) rock.

FIGURE 30. Rock outcrop of sandstone.

Granodiorites (Carboniferous?) are located next to the Sangiin Dalai Nuur fault (Plate 1). Figure 31 and 32 were taken in close proximity to one another.

FIGURE 31. Picture of the granodiorite (Carboniferous?) with no foliation.

Sandy schist, is located in the north, east, and the southeast of the map (Plate 1). Seventy percent of the schist samples have quartz veins (Figure 33).

FIGURE 32. Picture of the granodiorite (carboniferous?) with some foliation.

FIGURE 33. Rock outcrop of the sandy schist this rock sample has been highly fractured.

Volcanogenic schists are located in the middle of map extending from the southeast corner to the north edge of the map (Plate 1, Figure 34).

FIGURE 34. Rock outcrop of schist.

Siliceous terrigenous rocks are located just northeast of the center of the map, northwest, and southwest (Plate 1). These rocks have experienced small to large degree of metamorphism. The samples include fine to coarse-grained sandstone interbedded with slate and phyllite. The sandstone is light gray in color and weathers a tan brown. Forty percent of these samples had quartz veins (Figure 35, 36, and 37).

FIGURE 35. Sandstone rock in the silicous terrigenous rock terrane.

FIGURE 36. Phyllite outcrop in the siliceous terrigenous rock terrane.

FIGURE 37. Rock outcrop of slate in the siliceous terregenous rock terrane.

Sandstone aleurolite are located from the southeast extending to the upper southwest side of the map (Plate 1). The sandstones have experienced a small amount of metamorphism. The unit is fine to coarse-grained sandstone with interbedded shale. The sandstone weathers light brown to orange and the fresh surface is gray blue (Figure 38 and 39).

The following figures below include the data recorded from the field. Each of the maps displays the recorded data measured in the field. These data consist of strike and dips, foliations, and cleavages, (Figure 40 to 42, respectively). The foliations and cleavages measurements were taken of metamorphic rocks which include phyllite and schist.

FIGURE 38. Picture of the sandstone.

FIGURE 39. Rock outcrop of the sandstone aleurolite.

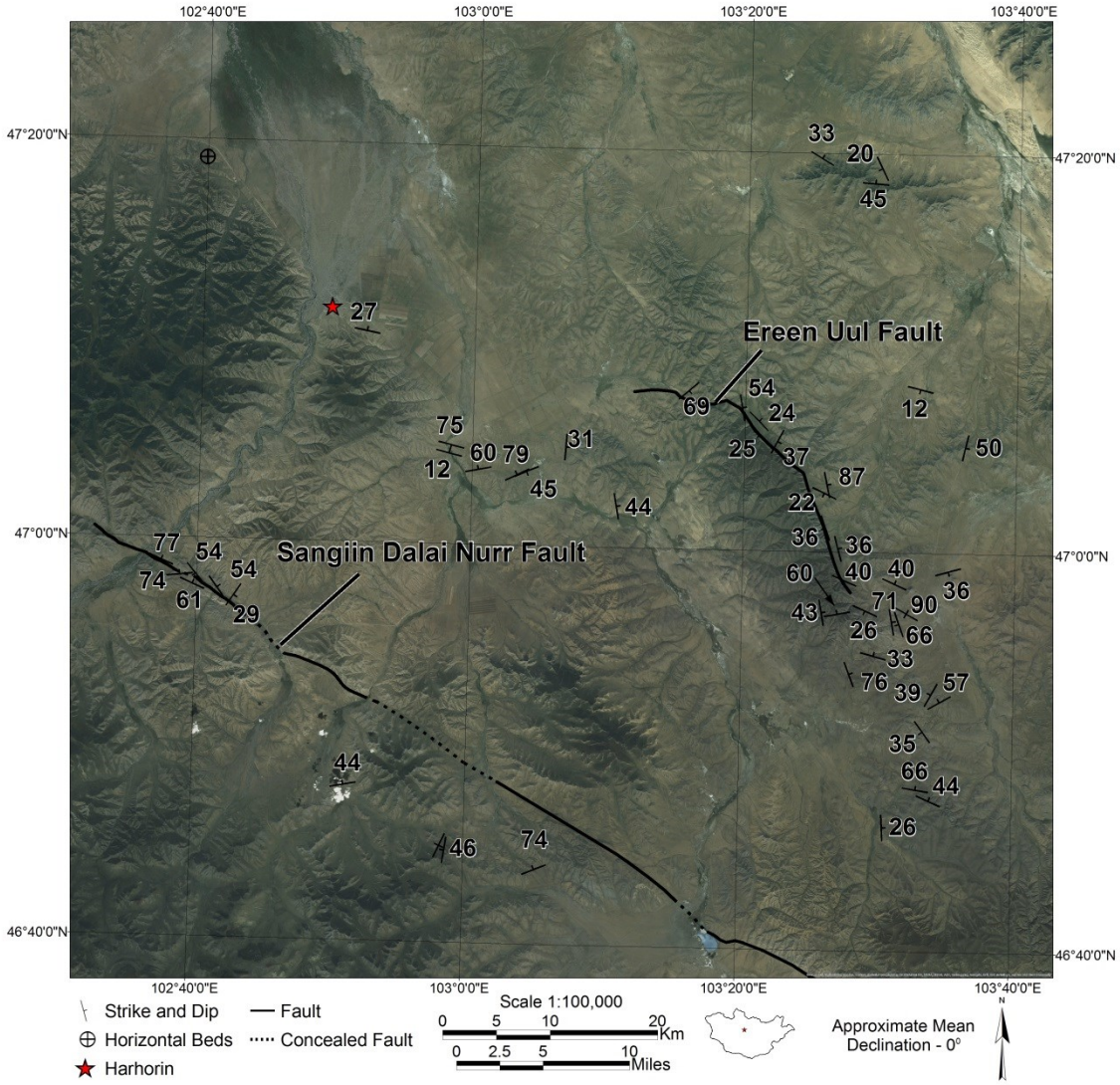

FIGURE 40. Strike and dip measurements (some measurements omitted due to spacing of data).

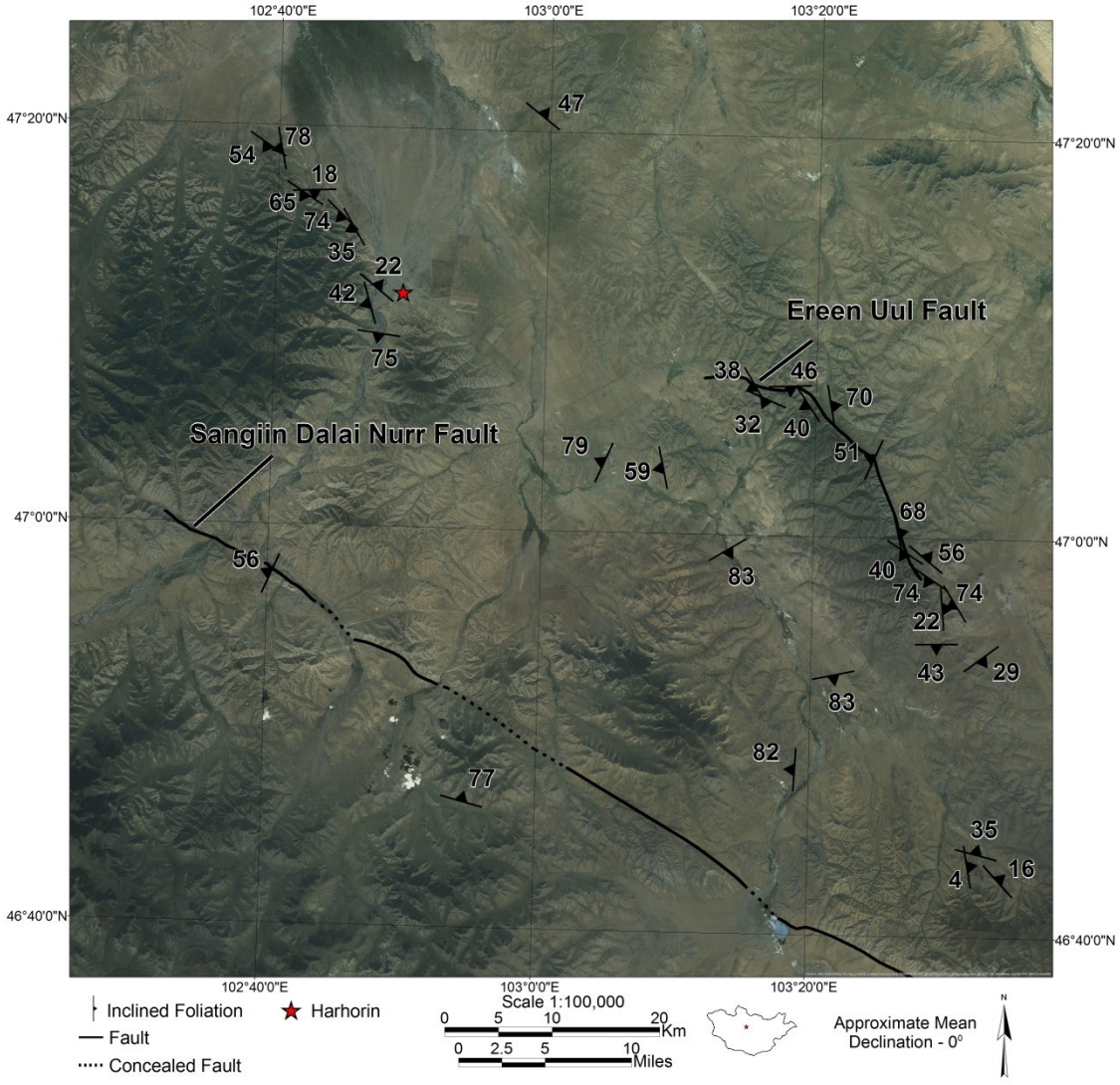

FIGURE 41. Representative foliation measurements (some measurements omitted due to spacing of measurements).

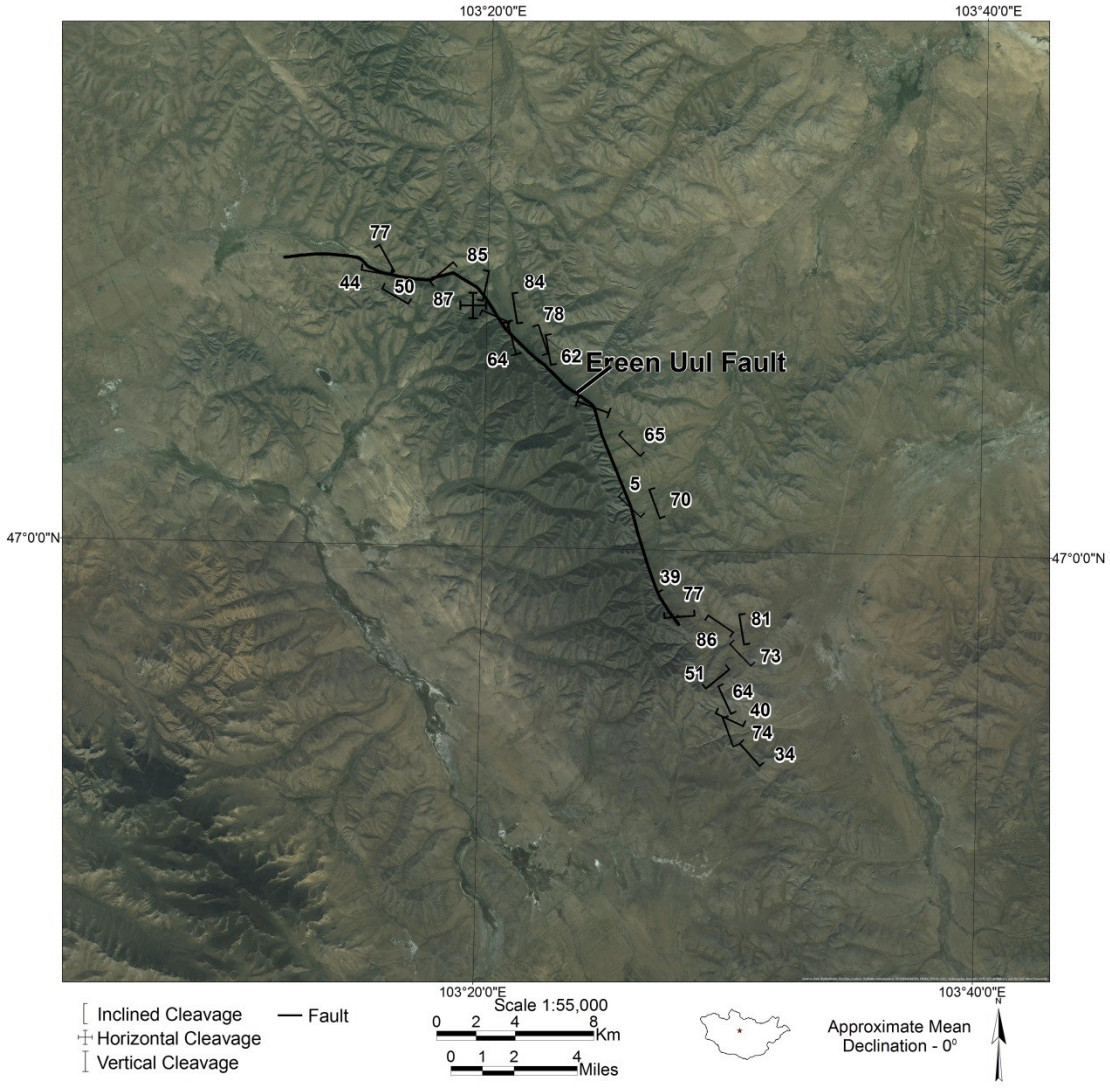

FIGURE 42. Representative cleavage measurements (some measurements omitted due to spacing of measurements).

The cleavage measurements taken near the Ereen Uul fault were plotted on a stereonet to observe the distribution of data and examine trends (Figure 43). Three trends in the data are worth noting. These trends have of strike of 280 with a dip of 45 degrees

to the southwest, a strike of 51 with a dip of 85 degrees to the northwest, and a strike of 160 with a dip of 79 degrees to the northeast.

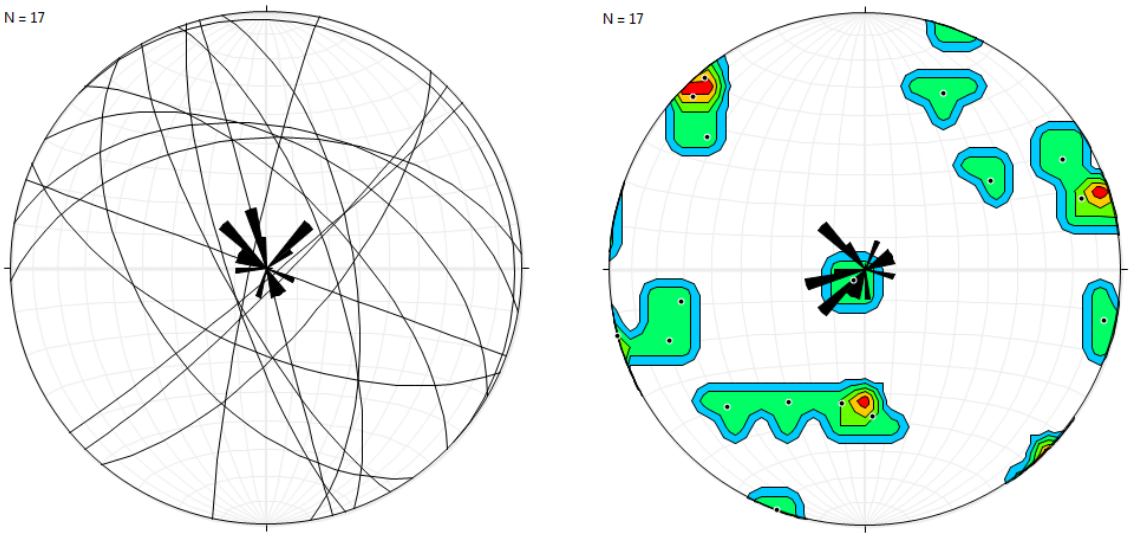

Figure 43. Stereonet displaying the cleavage measurements next to the Ereen Uul fault. The rose diagram to the left has a max value of 11.76% between 41 and 50 degrees. The mean vector is 331.4 degrees. The poles to the planes are plotted in the right image along with a 1% area contour around these points, the contour interval is 2%. The rose diagram has a max value of 11.76% between the 221 to 230 degrees, the mean vector is 241.4 degrees. This data was collected next the Ereen Uul Fault.

Foliation data points near the Ereen Uul fault were plotted on a stereonet (Figure 44). There are two concentrations of points in the data; one that ranges in strikes from 152 to 88 with a dip that ranges from 100 to 97 degrees to the northwest and the other strikes approximately 350 degrees with a dip of 27 degrees to the southwest.

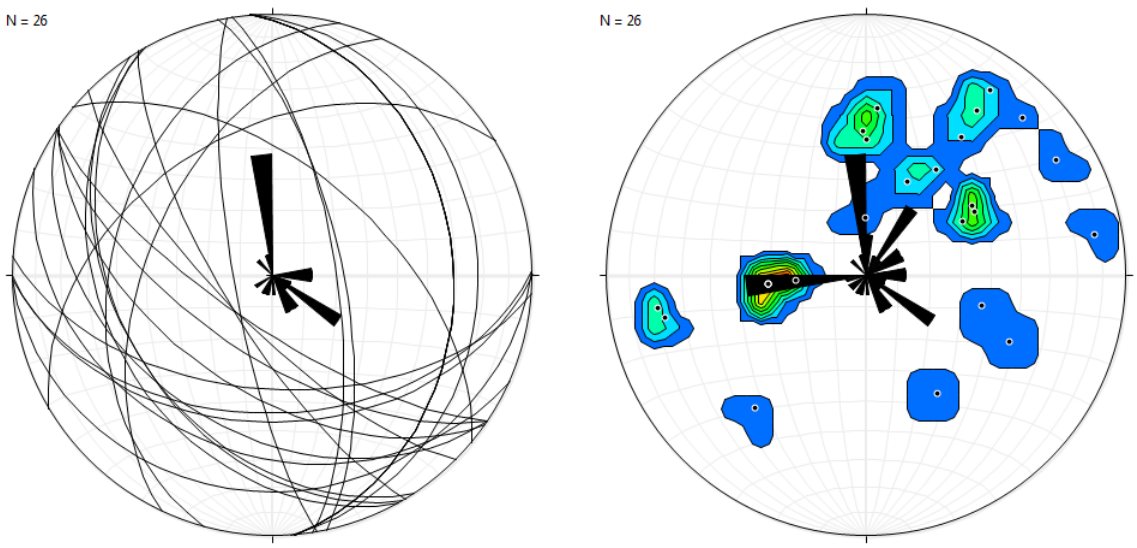

Figure 44. Stereonet displaying the foliation measurements next to the Ereen Uul fault. The planes are plotted to the left and it shows that the max value is 23.07% between 351 to 360 degrees. The mean velocity is 108.0 degrees. The poles to the planes are plotted in the image to the right. These pols are contoured with a 1% area contouring. The max value is 23.07% between 361 and 270 degrees and the mean velocity is 279.6 degrees.

The strike and dip measurements taken next to the Ereen Uul fault are plotted in Figure 45. Eleven strike and dips were measured. There are two main trends in the data, one with a strike that ranges from 116 to 170 with a dip that ranges from 22 to 55 degrees to the southwest and the other which has a strike that ranges from 350 to 313 with a range in dip from 25 to 54 degrees to the northwest. Strike and dip measurements were taken next to the Sangiin Dalai Nurr fault (Figure 46). There is a concentration of poles to planes in the south west hemisphere. One red location represents a strike of 333 degrees with a 58 degree dip to the northeast while the other represents a strike of 290 degrees with a dip of 75 degrees to the northeast.

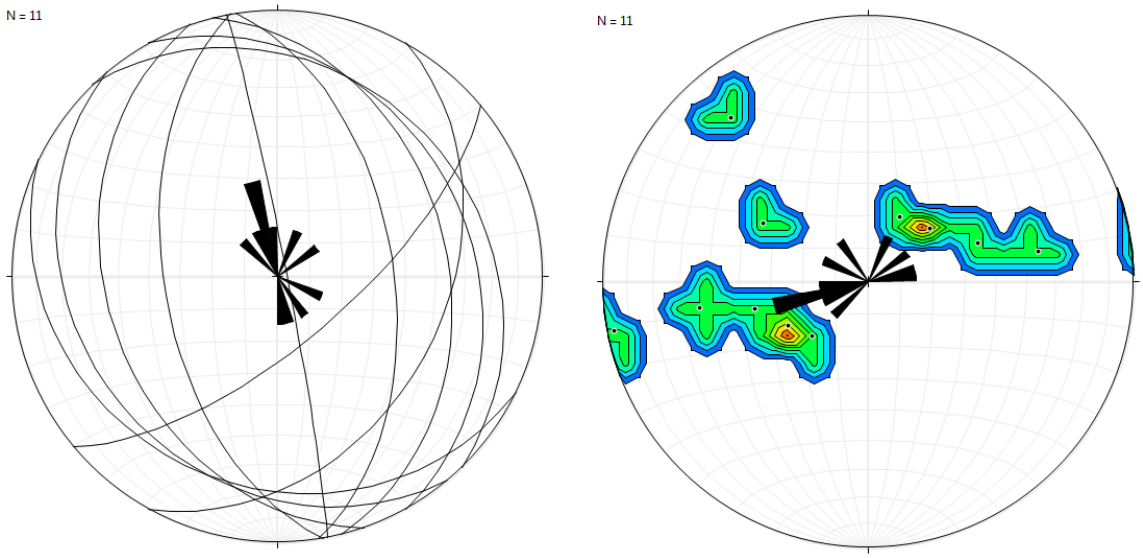

FIGURE 45. Stereonet net displaying the strike and dip measurements along the Ereen Uul fault. The rose diagram on the left shows that a max value of 18.18% between 341 and 350 degrees with a mean vector of 27.6 degrees. The image to the right shows 1% area contouring of the poles to the plains. The contour interval is 2% with the counting area 1% of the net area. The rose diagram shows a max value of 18.8% between 251 and 260 degrees with a mean vector of 297.6 degrees.

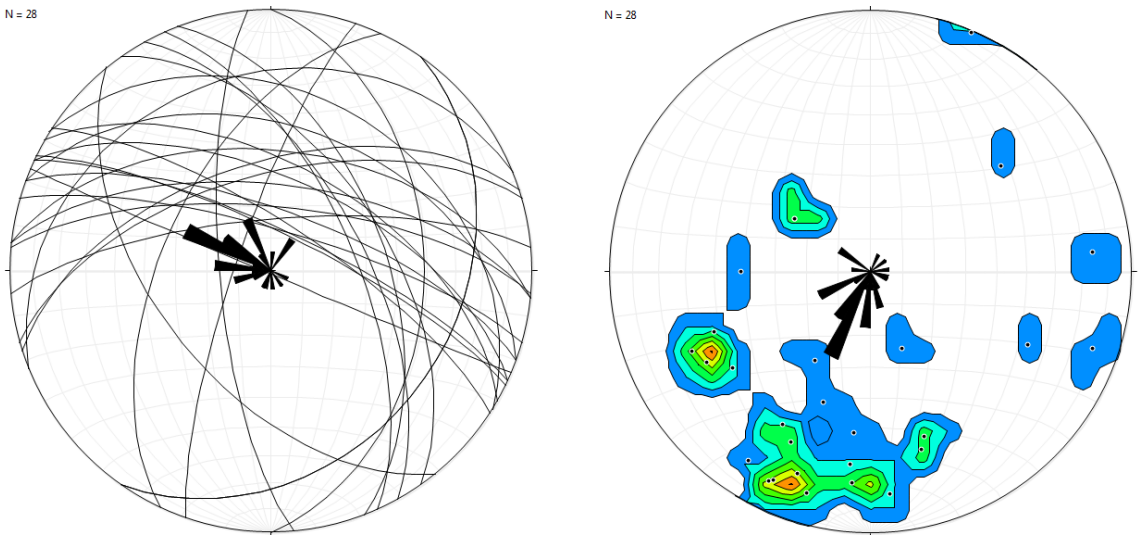

FIGURE 46. Stereonet net displaying the strike and dip measurements along the Sangiin Dalai Nurr fault. This data was taken at 28 locations which includes data form the north and south sides of the fault. The plot to the left represents the strike plane and the corresponding rose diagram. The rose diagram shows that the max value is 17.86% between 291 and 300 degrees with a mean vector of 289.6 degrees. The plot to the right represents the poles to the planes. These poles were contoured using 1% area. Each contour interval is 2%. The rose diagram has a max value of 17.85% between 201 and 210 degrees with a mean vector of 199.6 degrees.

Remote Sensing

False Color Images

In this section the remote sensing images used to evaluate the Ereen Uul fault and the Sangiin Dalai Nuur fault are shown. Figure 47 shows the entire satellite image from

the USGS and Figure 48 displays the area that includes the two faults and the city of Harhorin.

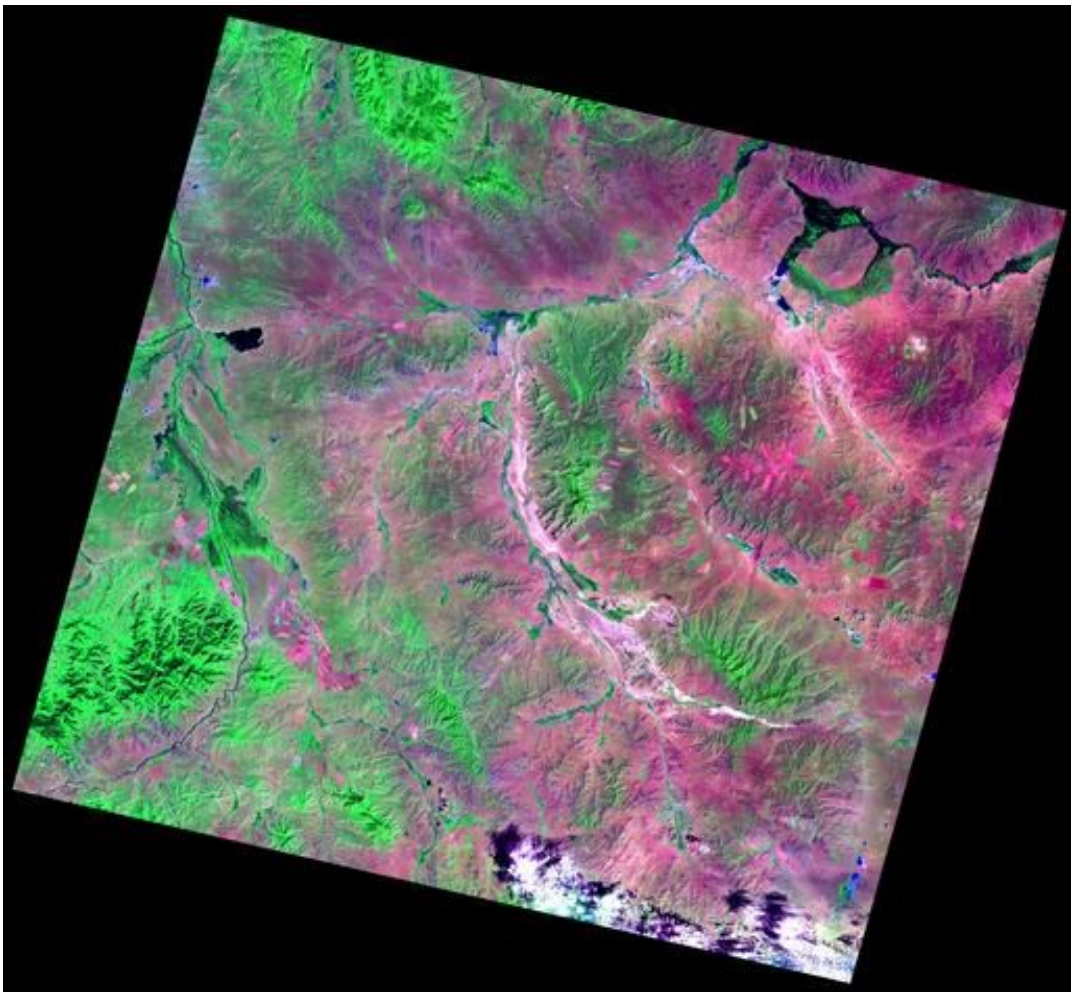

FIGURE 47. Landsat 7, 7-4-2 satellite image showing a portion of central Mongolia.

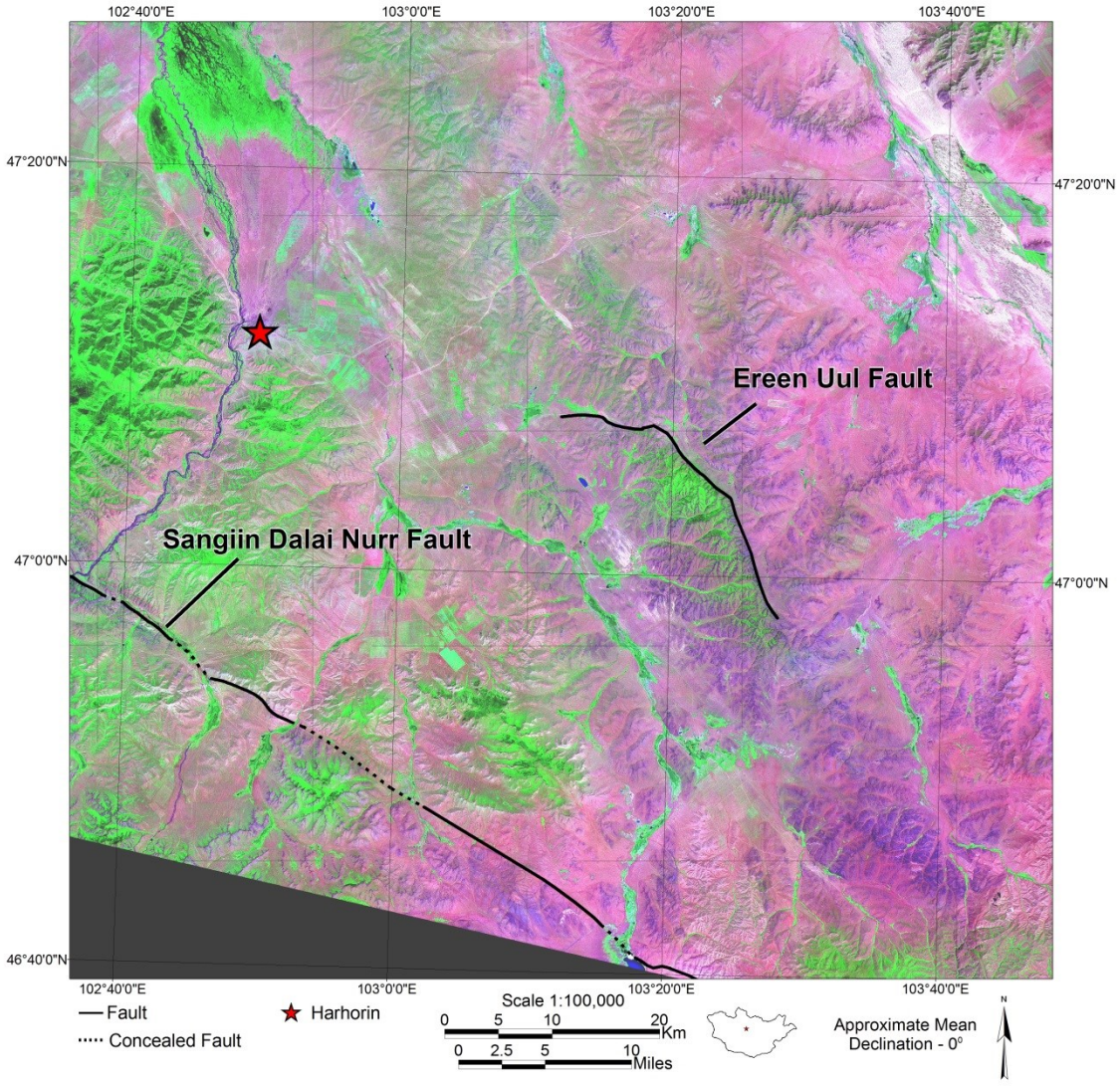

FIGURE 48. Landsat 7, 7-4-2 satellite image showing the location of the Ereen Uul Fault, Sangiin Dalai Nuur Fault, and the city of Hahorin. The two faults are labeled and the city is a red star on the map.

Digital Elevation Model

Digital Elevation Models (DEM) are 3D representations displayed as a raster images. DEMs show the topography and are helpful in locating linear features such as

faults. DEMs can be used to find drainage basins and analyze geomorphic indices. Figure 49 shows the DEM and the two faults that was used for analysis.

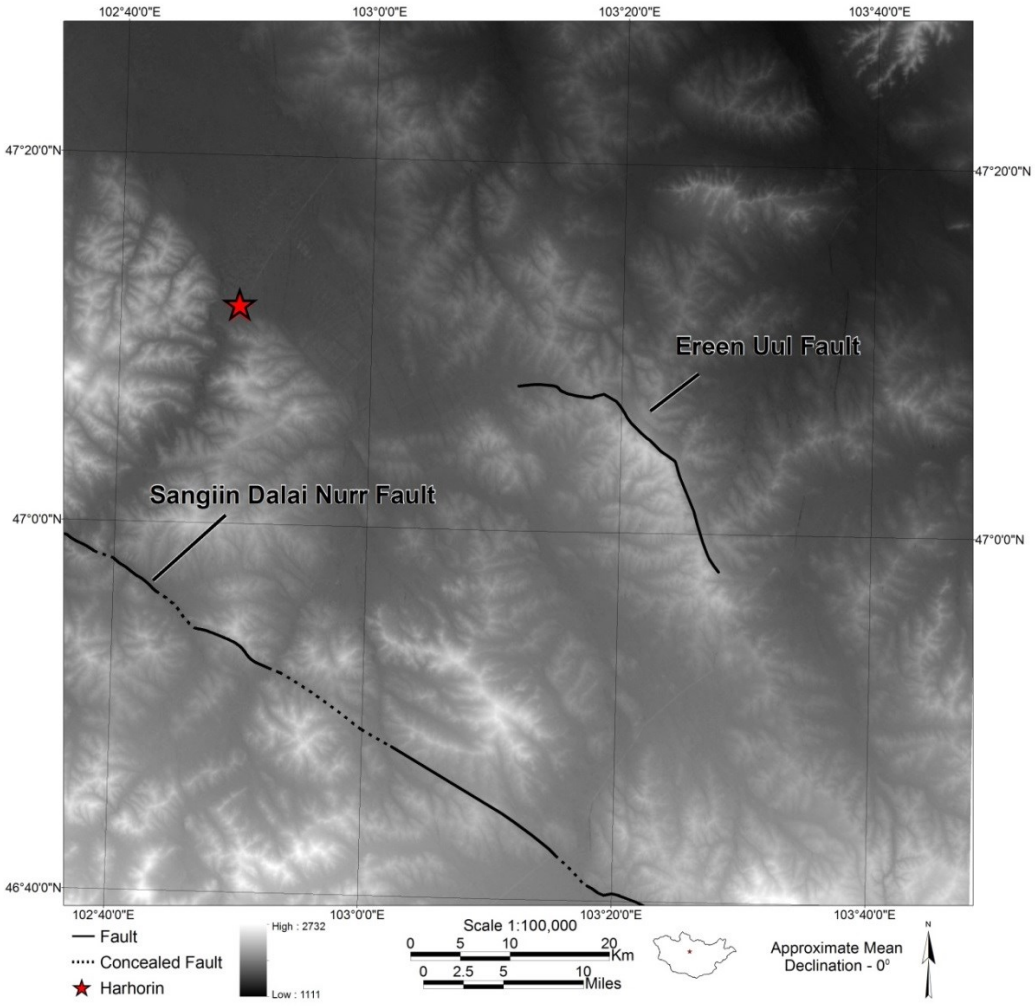

FIGURE 49. DEM image of the field area, showing Harhorrin for reference and the locations of the faults.

Geomorphic Indices

The DEM was analyzed in ArcGIS to determine the hypsometry, asymmetric mountain range, and stream length-gradient index of the areas next to the two faults of

interest. Figure 50 and 51 show elevation contours for the basins studied. Figure 52 shows the area of the drainage basins next to the Ereen Uul fault. The areas of the drainage basins on the west side of the mountain were compared to the basins on the east side. It was found that the basins on the east side were less than 10% of the size of the basins on the west side. For example, Basin 1 has an area of 51.1 km^2 and Basin 1a has an area of only 0.3 km^2 (Figure 52). This indicates that the mountain range is lifting asymmetrical with a faster rate of uplift on the east side.

Hypsometric curves were graphed for each of the basins studied. These curves show the distribution of the elevation across the basins and are normalized so they can be compared to each other. The hypsometric curves are included in Figures 53 to 59. The curves in these figures compare similar with each other for both the basins next to the Ereen Uul fault and for the basins next to the Sangiin Dalai Nuur fault.

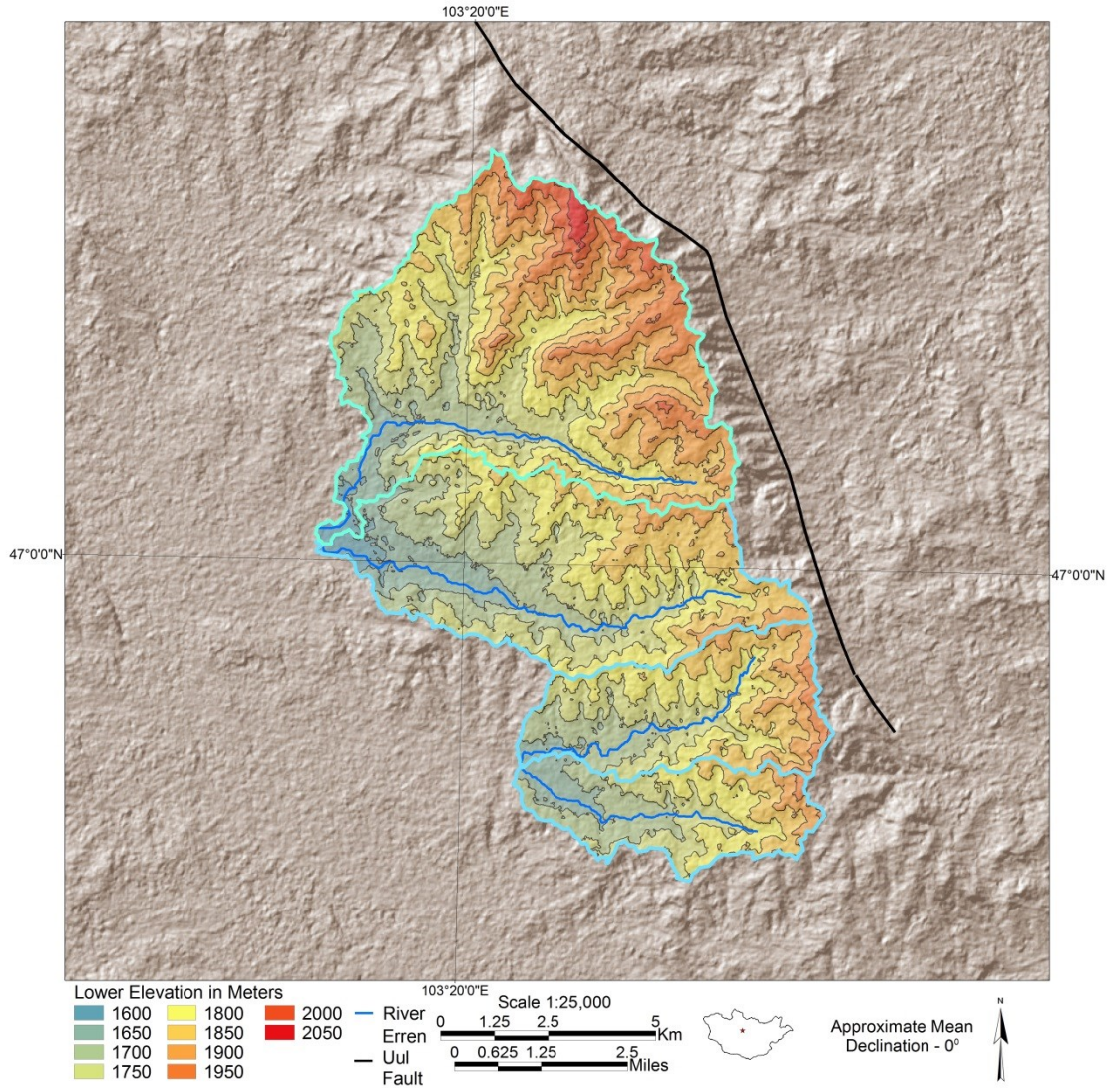

FIGURE 50. Hillshade image showing elevation contours of basins along the Ereen Uul fault.

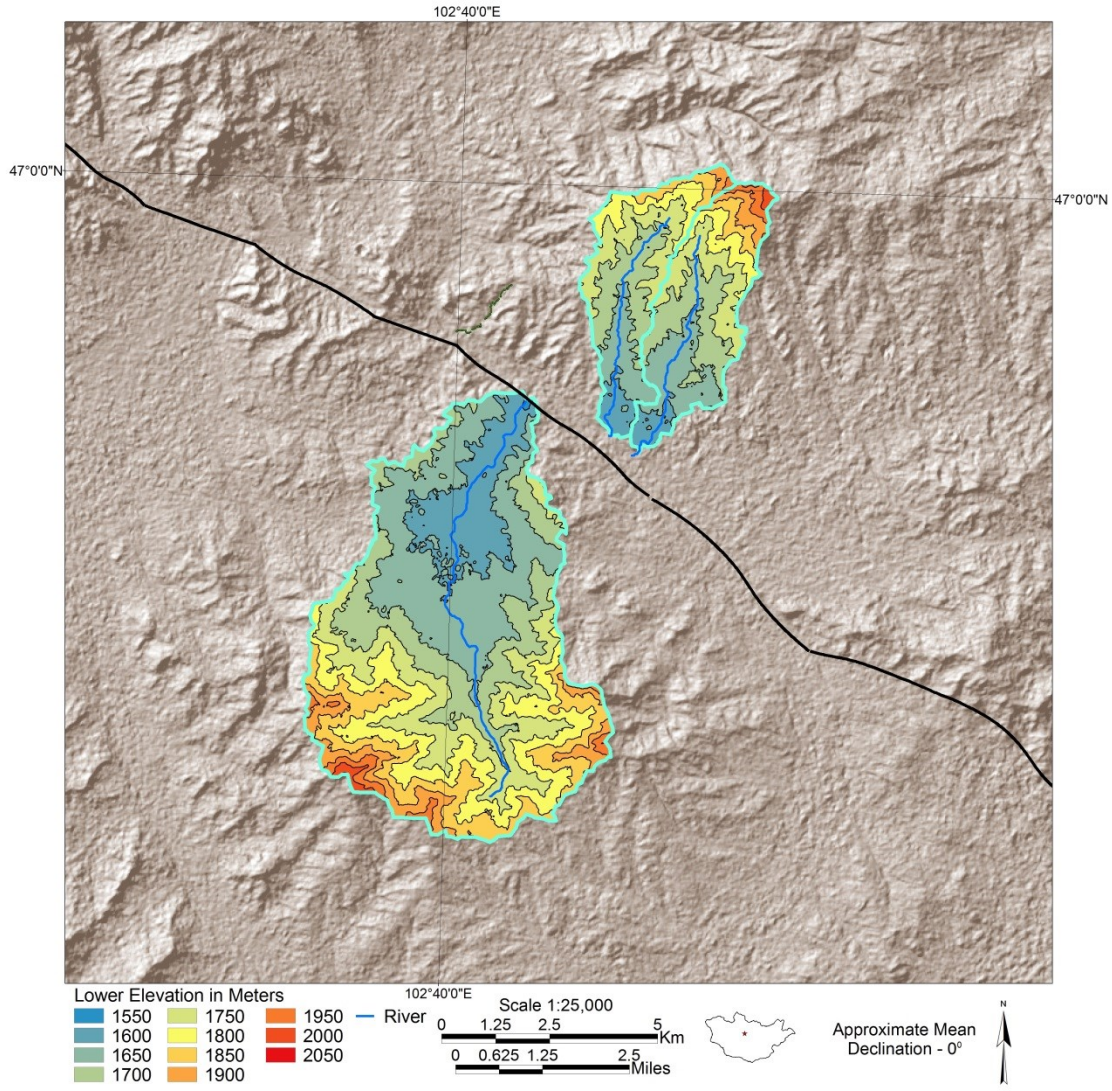

FIGURE 51. Hillshade image showing elevation contours of basins along the Sangiin Dalai Nuur fault.

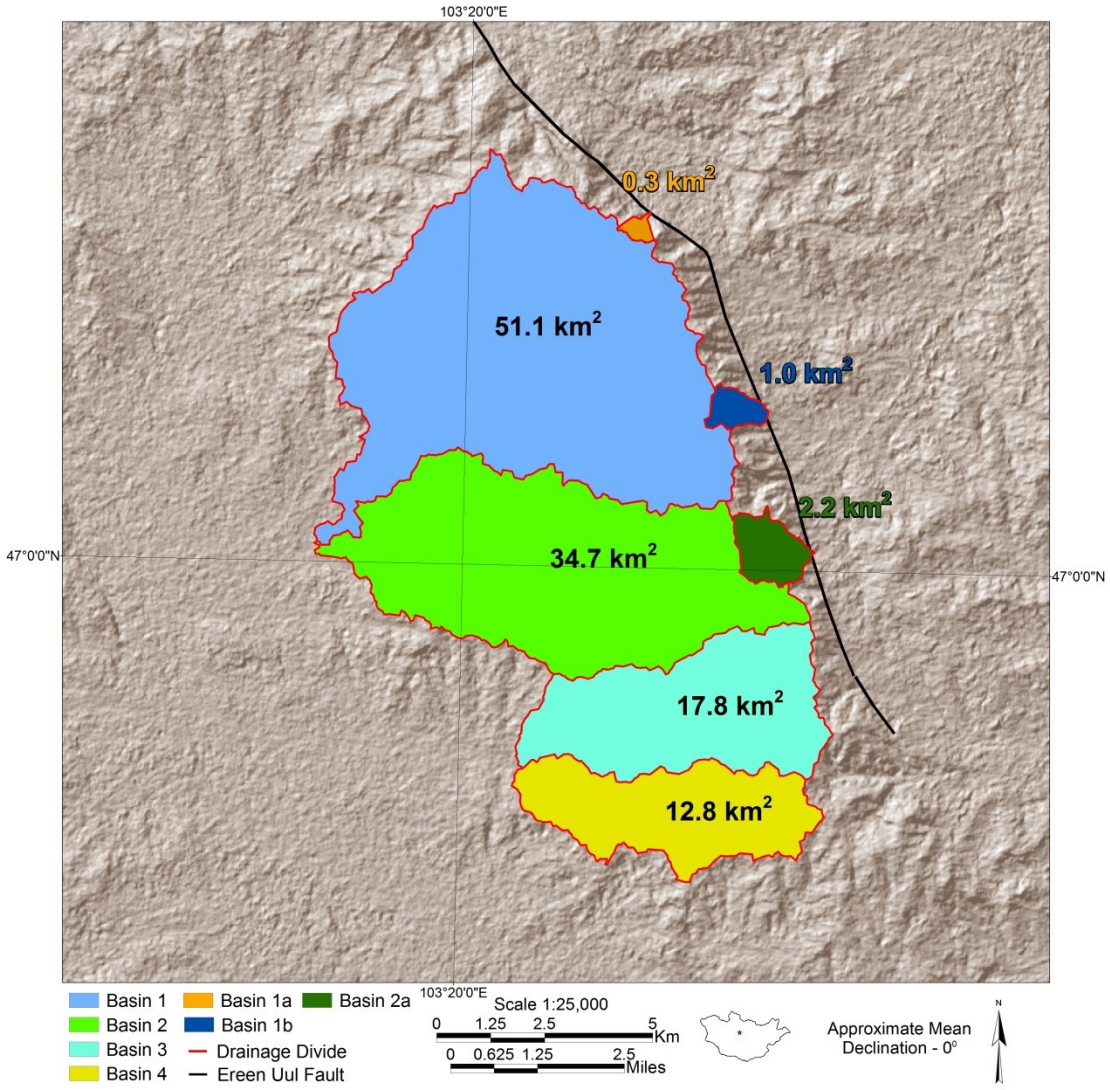

FIGURE 52. Asymmetric mountain range along the Ereen Uul Fault.

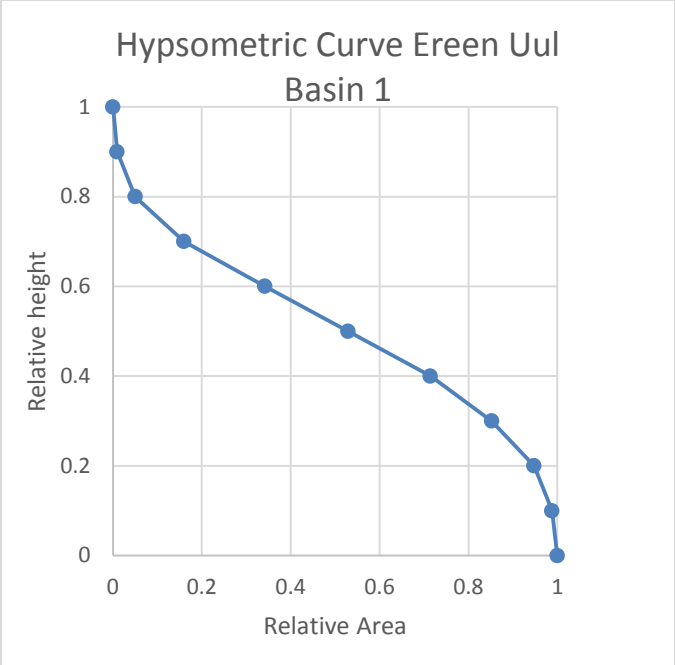

FIGURE 53. Hypsometric Curve of Ereen Uul Basin 1.

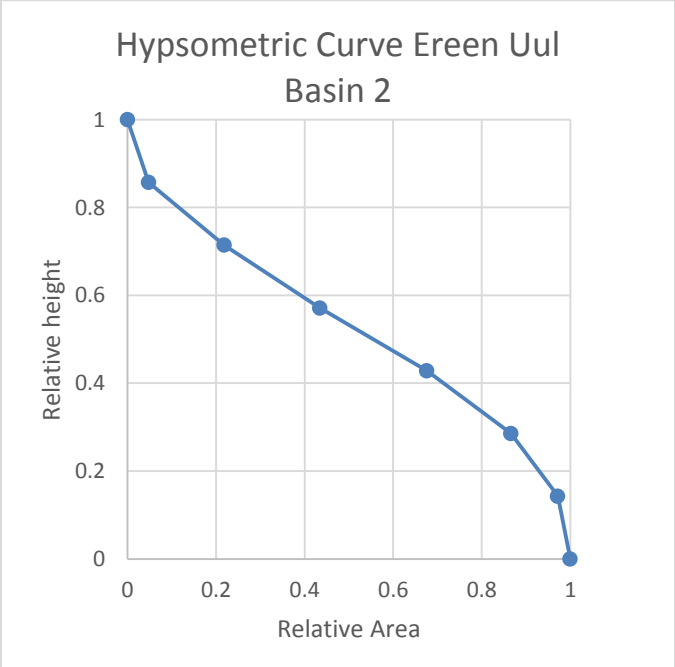

FIGURE 54. Hypsometric Curve of Ereen Uul Basin 2.

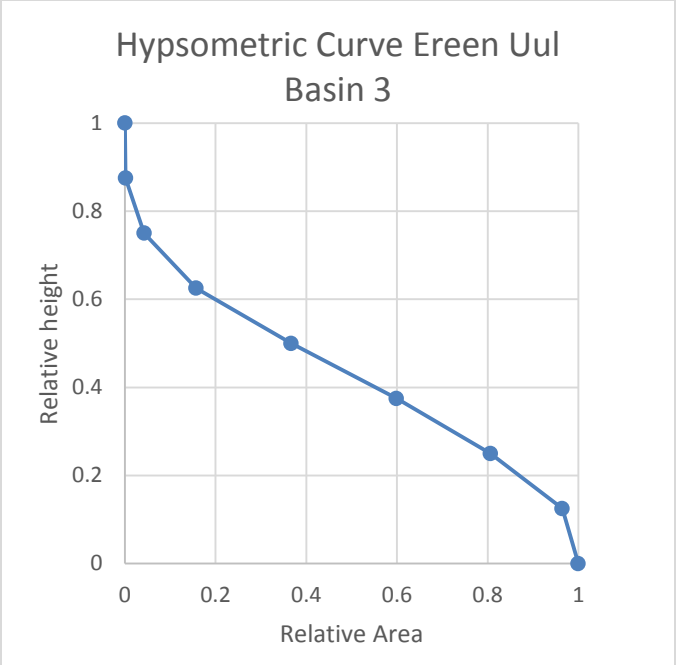

FIGURE 55. Hypsometric Curve of Ereen Uul Basin 3.

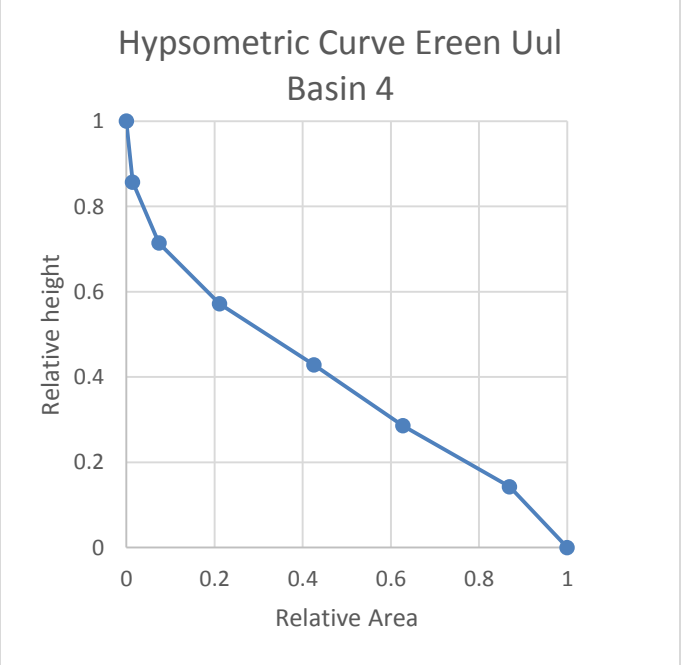

FIGURE 56. Hypsometric Curve of Ereen Uul Basin 4.

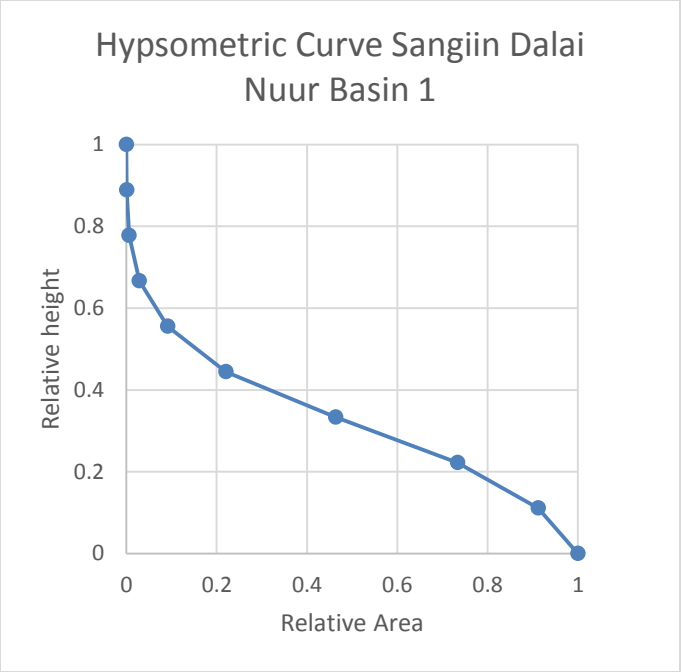

FIGURE 57. Hypsometric Curve of Sangiin Dalai Nuur Basin 1.

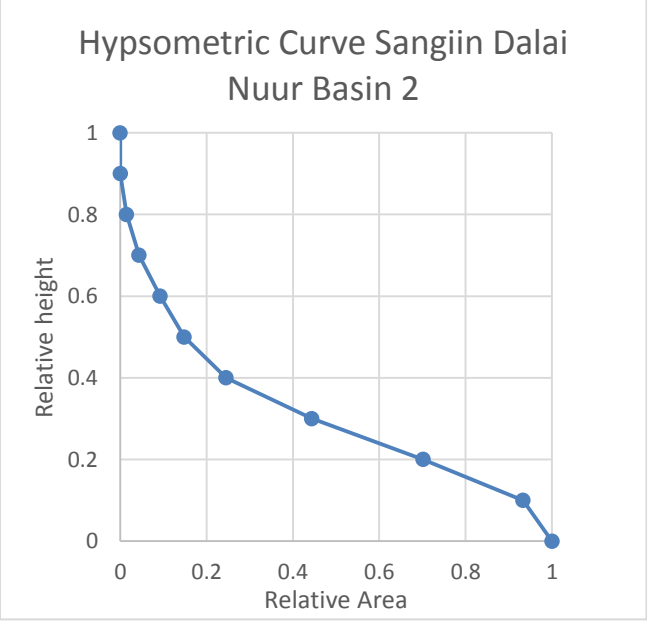

FIGURE 58. Hypsometric Curve of Sangiin Dalai Nuur Basin 2.

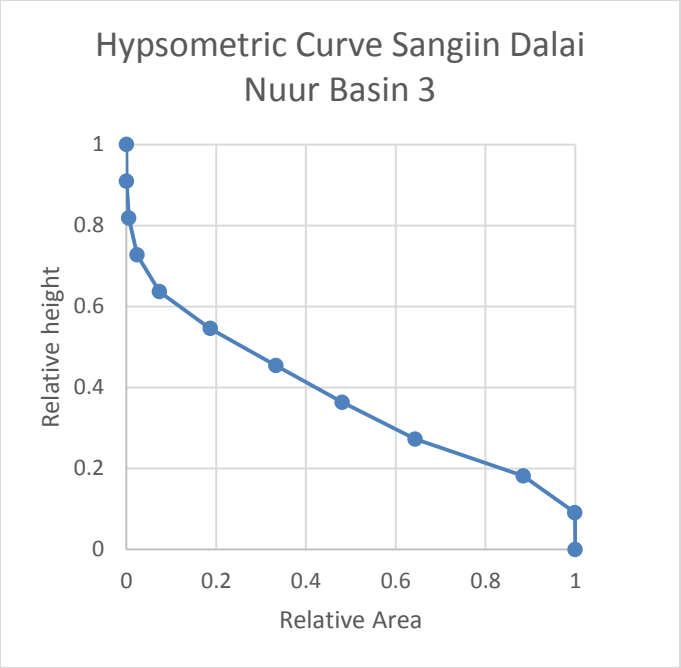

FIGURE 59. Hypsometric Curve of Sangiin Dalai Nuur Basin 3.

Stream profiles were created for each of the streams in the basins studied. The stream profiles along with the SL index calculated for each 50 foot contour are displayed in the graphs below (Figures 60 through 66). Some contour intervals only have a few data points and thus the SL index is not calculated for them. Due to the resolution of the DEM there are some jumps, falls and flat lines within the profiles.

An elevation profile was also created across the mountain next to the Ereen Uul fault. This profile shows the topography is steeper on the east side of the mountain next to the Ereen Uul fault compared to the west side of the mountain (Figure 67).

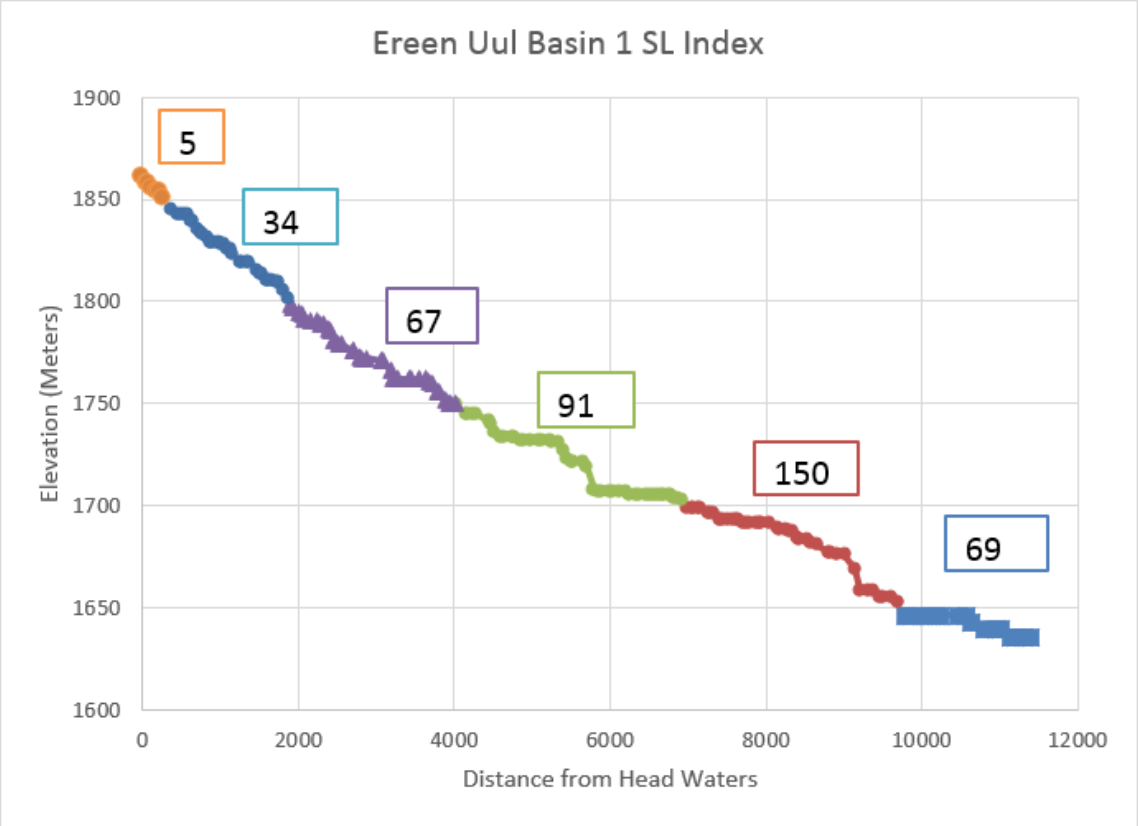

FIGURE 60. Stream profiles and SL Indices of Ereen Uul Basin 1.

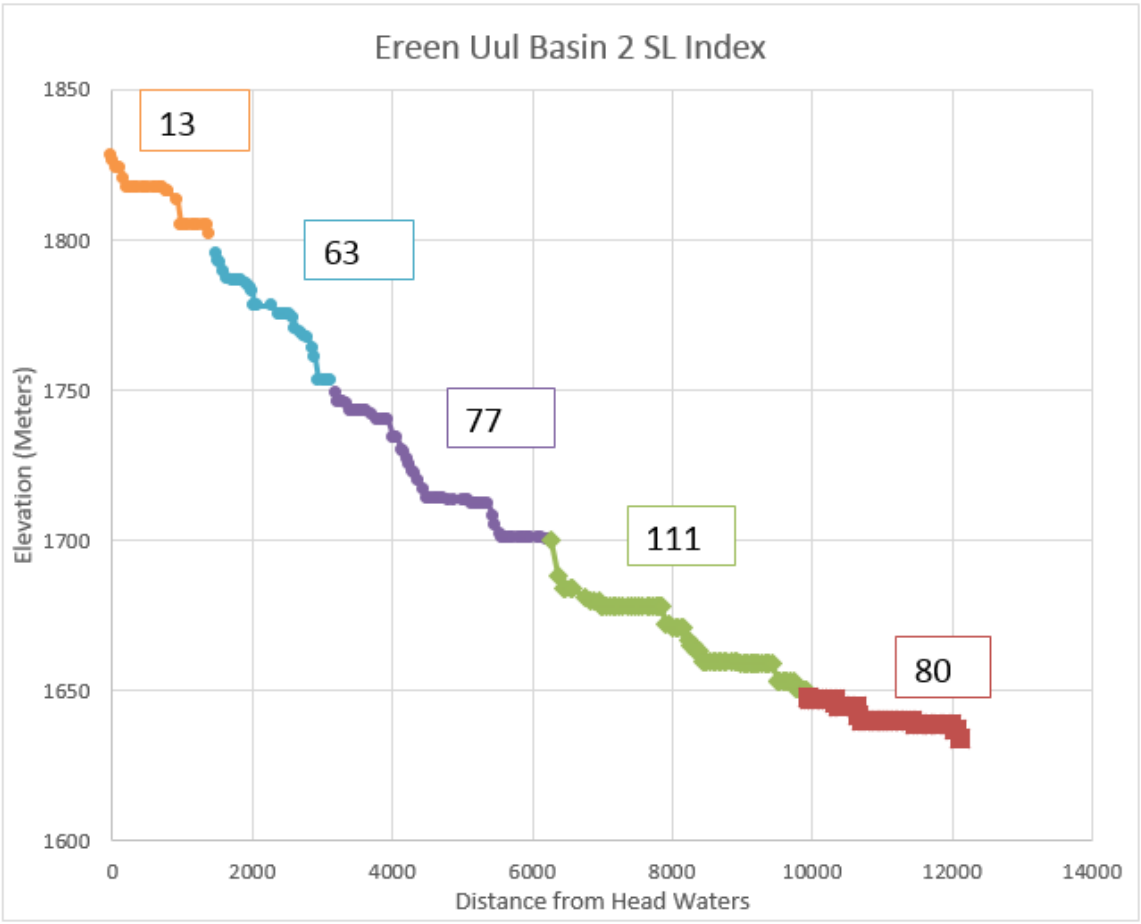

FIGURE 61. Stream profiles and SL Indices of Ereen Uul Basin 2.

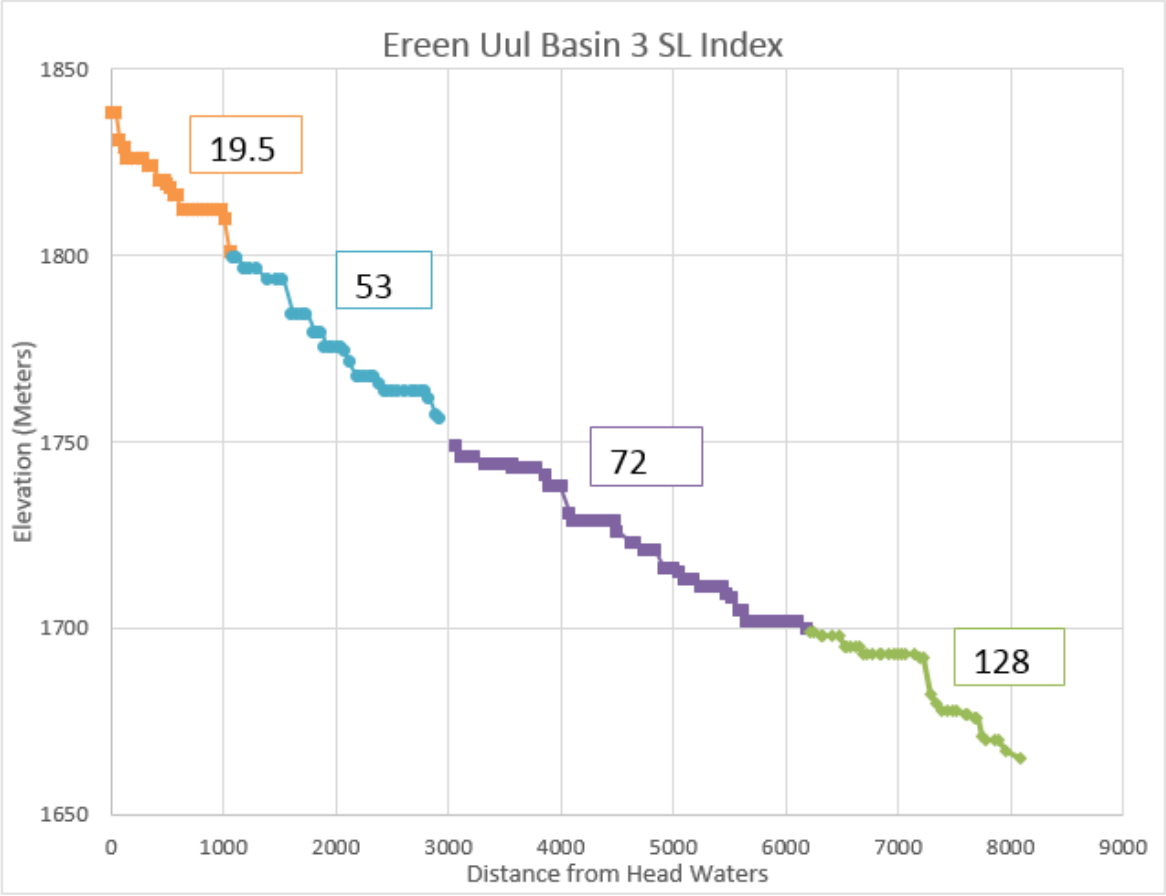

FIGURE 62. Stream profiles and SL Indices of Ereen Uul Basin 3.

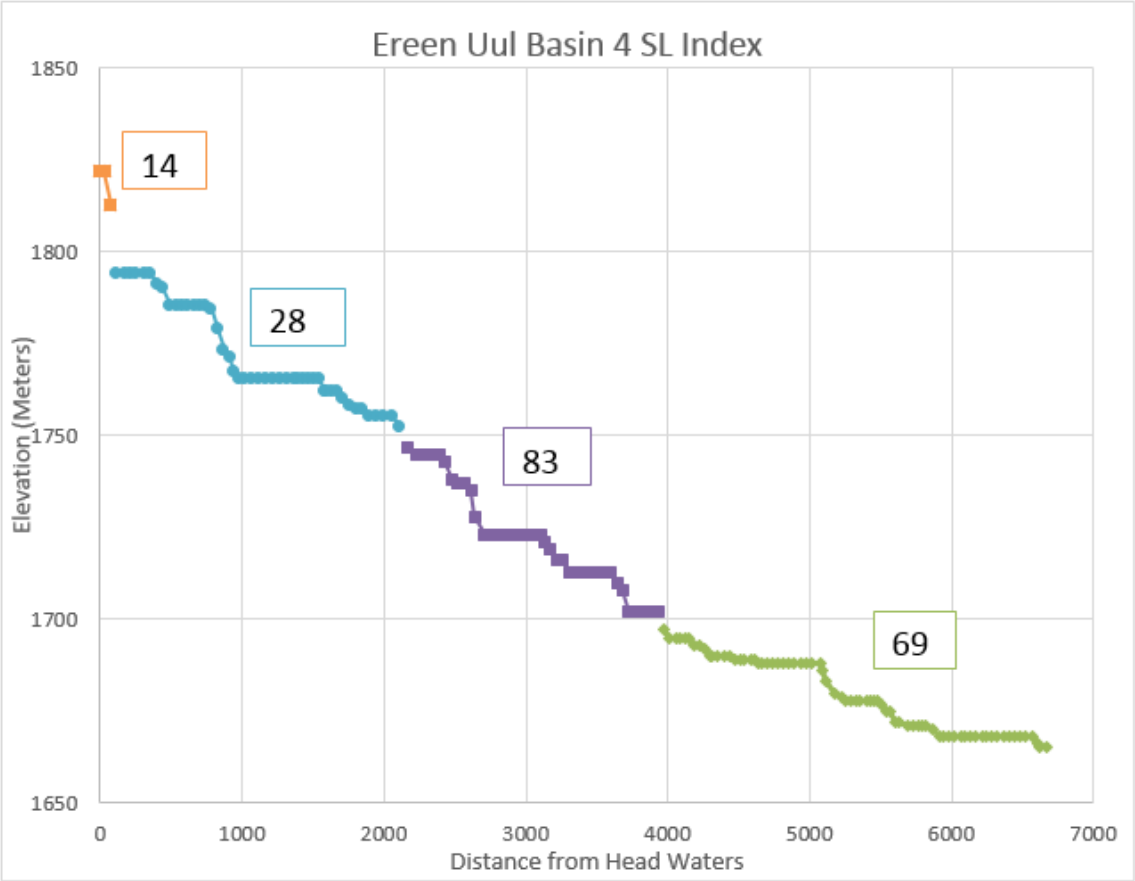

FIGURE 63. Stream profiles and SL Indices of Ereen Uul Basin 4.

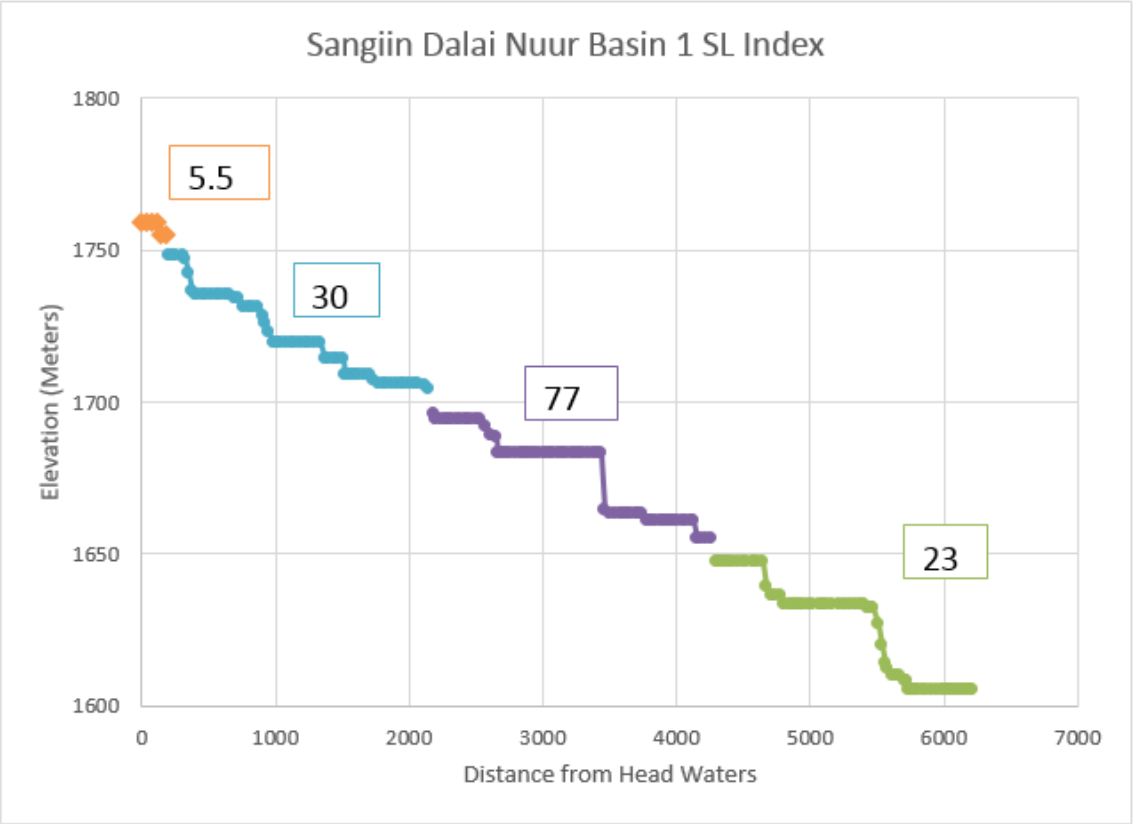

FIGURE 64. Stream profiles and SL Indices of Sangiin Dalai Nuur Basin 1.

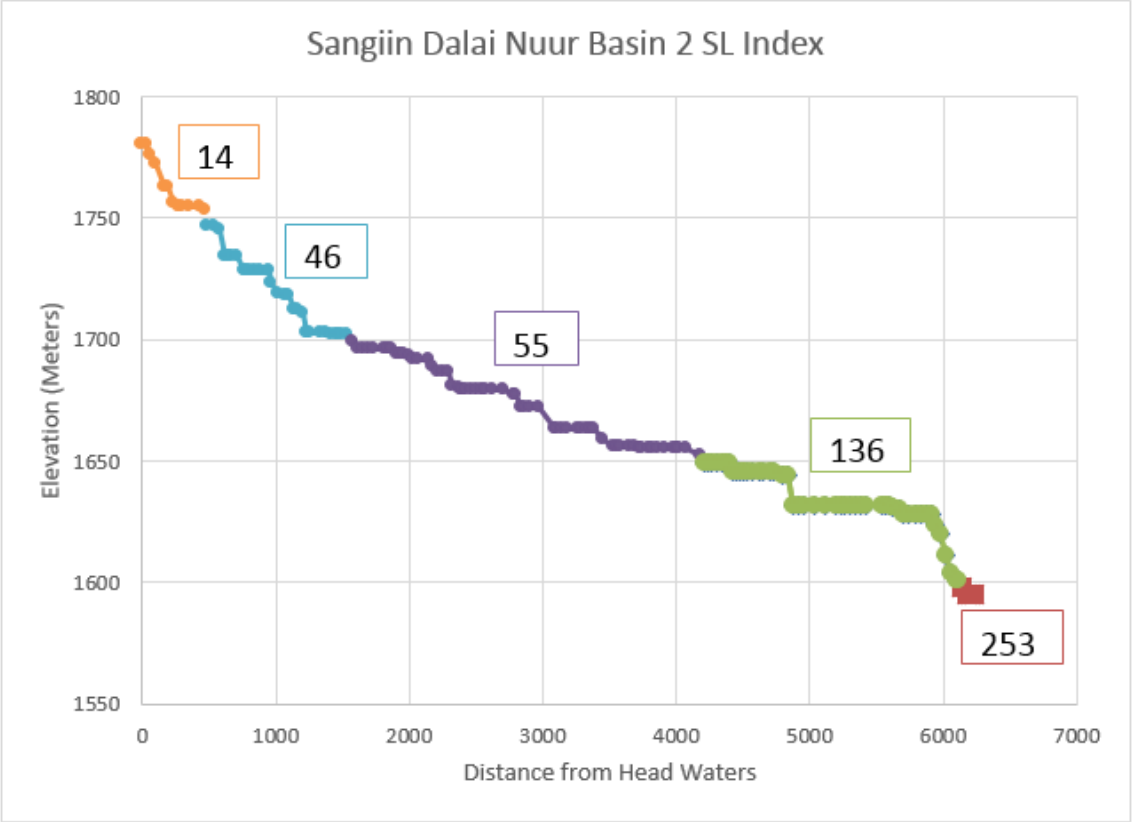

FIGURE 65. Stream profiles and SL Indices of Sangiin Dalai Nuur Basin 2.

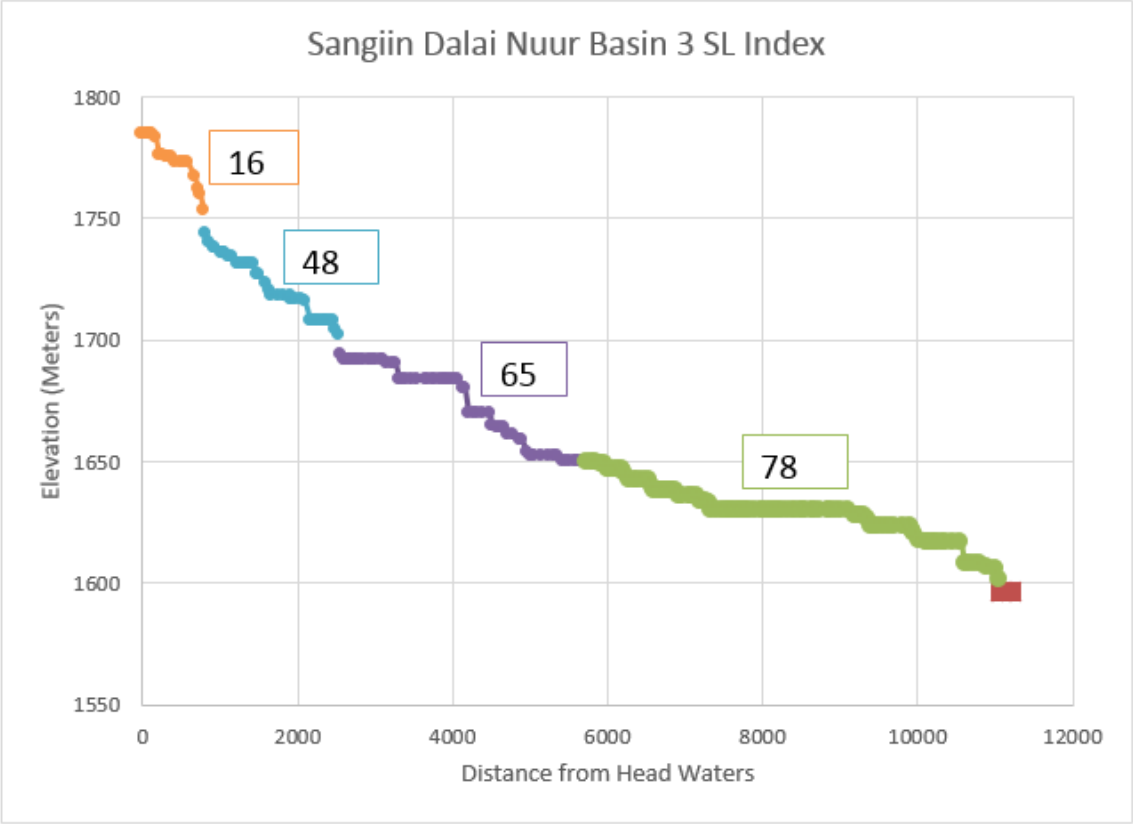

FIGURE 66. Stream profiles and SL Indices of Sangiin Dalai Nuur Basin 3.

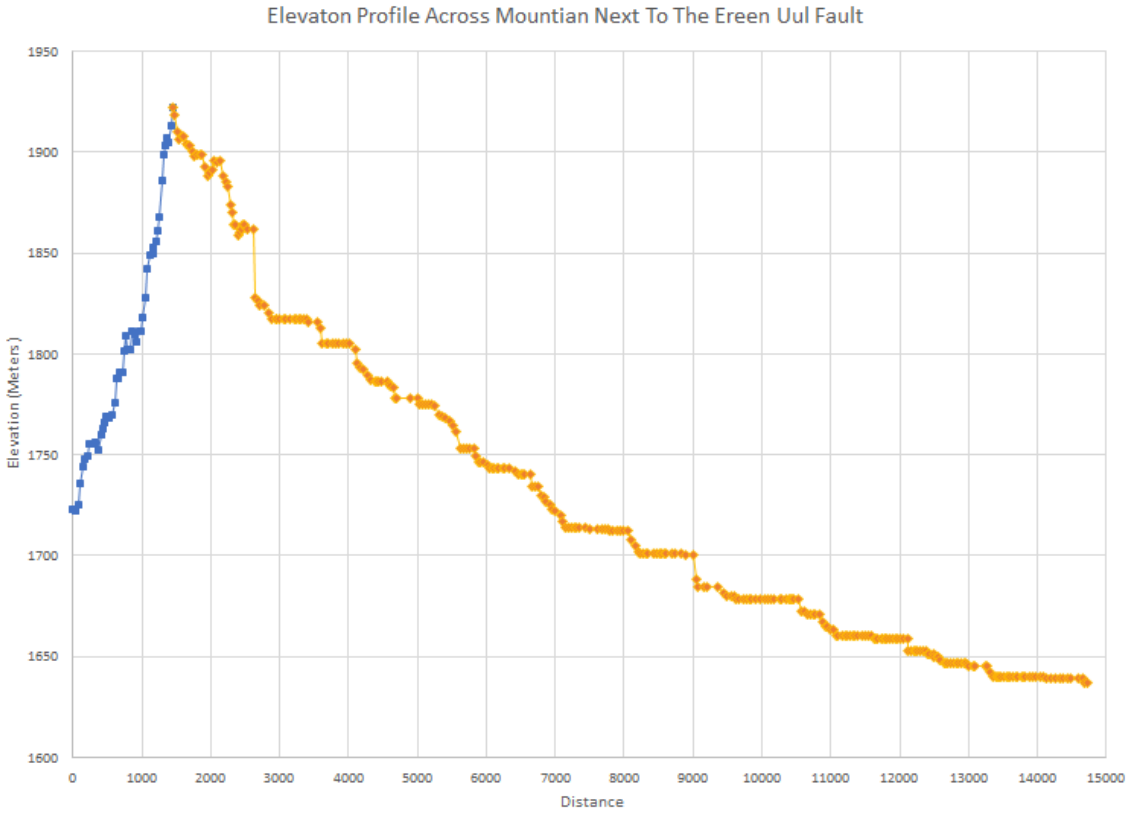

FIGURE 67. Elevation profile from east to west across the mountain next to the Ereen Uul fault. The east side of the mountain is steeper than the west side.

CHAPTER 5

DISCUSSION

Ereen Uul Fault

The Ereen Uul fault is located in the center of the map (Plate 1). The fault strikes N 20° W in the southern section, but bends to strike to N 45° W at approximately 47°03'55.52" N and 103°23'56.61" E. The dip along the fault is approximately 72° northeast (Figure 68). While mapping the Ereen Uul fault, several questions came up, including: What kind of fault is it? Why is there more topographic expression to the north and less to the south? Why is there a bend in the fault? How is this fault controlled by the regional tectonic stress?

What type of fault is it? The Ereen Uul fault is a normal fault. The mountain range next to the Ereen Uul fault is asymmetrical. The east side is steep and short while the west side is long and has a gradual slope. Normal faults are often bounded by asymmetric ranges (Burbank and Anderson, 2011). This asymmetric range can be seen when comparing the basins on either side of the mountain range. The drainage basins to the east are small compared to the basins to the west side. This difference in size indicates that the east side is uplifting at a much faster rate than the basin to the west. An elevation profile going from east to west shows that the east side is steeper than the west side (Figure 67).

FIGURE 68. Picture of the Ereen Uul Fault. The rocks to the left side of Tom are moving up. The picture is looking towards the north.

Why is there more topographic expression towards the north than to the south? The mountain is still uplifting and this is noted by looking at the drainage basins. The drainage basins on the east side of the range increase in size going from north to south. This indicates that the mountain is uplifting at a faster rate towards the north than the south.

Why is there a bend in the fault? There are north-south striking right-lateral strike-slip faults to the east and west of the Ereen Uul Fault. As these faults move they create a shearing force which acts upon the fault. This stress may be expressed by a

counter-clockwise rotation centered at the kink. The Ereen Uul fault is in between these right-lateral strike-slip faults and these faults could be the driving forces that cause the Ereen Uul fault to bend.

Compare this fault to the regional tectonic stress? In Mongolia strike-slip faults that are striking in a north south direction are generally right-lateral strike-slip faults. That compares similarly with the faults located in the field area. There is a lot of compression in the north south direction due to the collision of India with Asia. This pressure is relieved by extensional forces as material moves out to the east. The Ereen Uul fault is oriented north south and is extending in the east west direction. Lake Bikal in Russia is also experiencing extensional forces. The fault is 550 km north of the field area and is oriented approximately in North to south and is extending in the east west direction. This behavior can be seen when looking at the focal mechanisms diagrams (Figure 22).

Sangiin Dalai Nuur Fault

The Sangiin Dalai Nuur fault strikes N 58° W and is located in the southwest part of the study area (Plate 1). The fault extends at least 105 km and is located on the eastern side of the Hangay Mountains (Figure 20) located approximately 25 km south of Harharin. While mapping the Ereen Uul fault, several questions come up, including: what direction is the fault slipping? Does the fault die out in the Hangay Mountains towards the west? Is there any uplift along the fault? How is this fault controlled by the regional tectonic stress?

What direction is the fault slipping? The Sangiin Dalai Nuur fault is a right-lateral strike-slip fault. There is stream offset along the fault with at least 1.3 km of right-lateral offset (Figure 69).

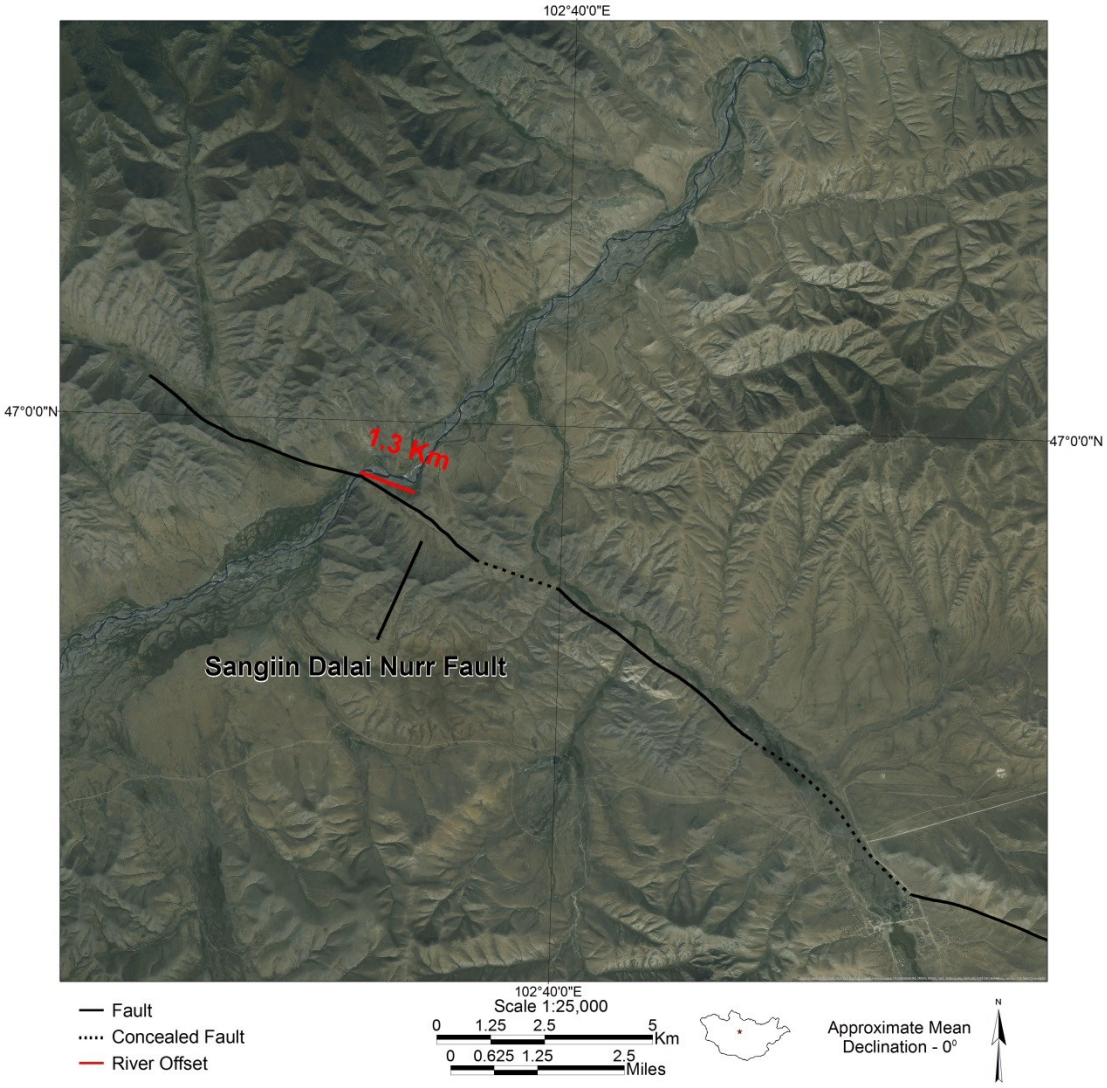

Figure 69. Stream offset along the Sangiin Dalai Nuur fault. The river is flowing from south to north. The offset along the stream is approximately 1.3 km, noted by the red line.

Does the fault die out in the Hangay Mountains towards the west? The Sangiin Dalai Nurr fault extends over 105 km and cuts across the entire field area. When looking at the satellite imagery it appears that the fault extends, past the river that is offset by the fault, into the Hangay Mountains approximately 11 km. This area was not visited in the field because there was no access across the river and was not included within the field area.

Is there uplift along the fault? There is no evidence for uplift along the fault. The hypsometric curve has been graphed for the Sangiin Dalai Nurr basins 1, 2, and 3 in (Figure 57, 58, and 59). The basins along the Sangiin Dalai Nuur fault appear to be mature. This indicates that the area is eroding rapidly or that it is not recently uplifting. The stream profiles and SL indices for the basins next to the Sangiin Dalai Nuur generally show no significant changes this indicates that faults are not presence within these basins and that there are not any significant changes in the weatherability of the bedrock.

How is the fault controlled by regional tectonic stress? The strike-slip faults in Mongolia that are oriented in a north south direction are generally right-lateral. As mentioned above there is a lot of compression in the north south direction. This compression causes right-lateral strike-slip faults throughout this area.

Geologic Timeline

The field area is composed mostly of meta-sedimentary rocks from the Devonian. These rocks are the oldest in the field area and were deposited around the same time as oceanic crust was being subducted underneath the Tuva Mongol Massif. This subduction

continued into the Jurassic period (Şengör and Natal'in, 1996). Compressional forces are evident because there are repeating devonian units in the field area. This subduction was also the cause for the intruding Carboniferous granites. These granites are located in the south-western half of the field area and cut the older Devonian meta-sedimentary rocks. These granites were later cut by Triassic-Jurassic aged granites. The Triassic-Jurassic intrusions are not as widespread in the field area and are located mostly in the south center section. As Mongolia was compressing in a north south directon strike-slip faults and normal faults began to form. The strike-slip faults in the field area are right-lateral strike-slip faults that are oriented in the north south direction. These faults cut the intruding granites and some of them are still active.

CHAPTER 6

CONCLUSIONS

Field observations and remote sensing was used in conjunction with geomorphic indicies to determine the activity of the Ereen Uul fault and the Sangiin Dalai Nuur fault. The Ereen Uul fault is a normal fault and has recent uplift on the eastern side of the range this can be seen when looking at the geomorphic indicies. The Sangiin Dalai Nuur fault is a right-lateral strike-slip fault and it is considered to be active because there is an offset stream that indicates recent movement along this fault.

A geologic map at a scale of 1:100,000 encompassing 8,072 km^2 was created for the field area in central Mongolia (Plate 1). This map was created using remote sensing, field investigation, and referenced two maps created by the Institute of Geology and Mineral Resources titled "Geologic Map of Mongolia at a scale of 1:1,000,000" (1998) and "Tectonic Map of Mongolia at a scale of 1:1,000,000" (2002). The map has updated contacts, fault lines, and for the first time, includes fault movement. A cross section was created that extends from the Sangiin Dalai Nuur fault to the Ereen Uul fault and shows a series of strike slip faults, one normal fault, and intrusive rocks (Plate 1).

PLATE

GEOLOGIC MAP

An electronic version of the geologic map is available as a supplemental file to this PDF in the ProQuest Dissertations and Theses database.

REFERENCES

REFERENCES

Ankhtsetseg, D., Adiya, M., Munkhuu, D., Selenge, L., and Tsembel, B., 2007, The seismicity in Mongolia: paper presented at 50th anniversary earthquake conference commemorating the 1957 Gobi-Altay earthquake, Ulaanbaatar, Mongolia, July 25 - August 8, 2007.

Badarch, G., Cunningham,W. D., and Windley, B. F., 2002, A new terrane subdivision for Mongolia: Implications for the Phanerozoic crustal growth of Central Asia: *Journal of Asian Earth Sciences*, v. *21* no. 1, p. 87-110.

Baljinnyam, I. Bayasgalan, A., Borisov, B. A., Cisternas, A., Dem'yanovich, M. G., Ganbaatar, L., Kochetkov, V. M., Kurushin, R. A., Molnar, P., Philip, H. Vashchilov, Y. Y., 1993. Ruptures of major earthquakes and active deformation in Mongolia and its surroundings: Geological Society of America, v. 181, p. 62

Buchan, C., Cunningham, D., Windley, B. F., and Tomurhuu, D., 2001, Structural and lithological characteristics of the Bayankhongor Ophiolite Zone, Central Mongolia: *Journal of the Geological Society*, v. 158, no.3, p. 445-460.

Burbank, D. W., and R. S. Anderson, R. S., 2011, References: Tectonic Geomorphology: Malden, Massachusetts, Blackwell Science, John Wiley & Sons, Ltd., p. 274

Byamba, J., 1990, Central and Eastern Mongolian geological map: Regional geological mapping division, Ulaanbaatar, Mongolia. (scale 1:500,000)

Cocks, L.R.M., and Torsvik, T. H., 2005, Baltica from the late Precambrian to mid-Palaeozoic times: The gain and loss of a terrane's identity: *Earth-Science Reviews*, v. 72, no. 1-2, p. 39-66.

Cunningham, W. D., 2001, Cenozoic normal faulting and regional doming in the southern Hangay region, Central Mongolia: Implications for the origin of the Baikal rift province: *Tectonophysics*, v. 331, no. 4, p. 389-411.

Delvaux, D., Moeys, R., Stapel, G., Melnikov, A., and Ermikov, V., 1995, Palaeostress reconstructions and geodynamics of the Baikal region, Central Asia, Part I. Palaeozoic and Mesozoic pre-rift evolution: *Tectonophysics*, v. 252 no.1–4, p. 61-101.

Didenko, A. N., Mossakovskii, A. A., Pecherskii, D. M., Ruzhentsev, S. G. Samygin, S. G., and Kheraskova, T. N., 1994, Geodynamics of the Central-Asian Paleozoic Oceans: *Russian Geology and Geophysics*, v.35, p. 48-61.

Enkin, R. J., Yang, Z., Chen, Y., and Courtillot, V., 1992, Paleomagnetic constraints on the geodynamic history of the major blocks of China from the Permian to the present: *Journal of Geophysical Research*, v. 97 no. b10, p. 13953-13989.

Institute of Geological and Mineral Resources., 1998, Geological Map of Mongolia Scale 1:1,000,000.

Institute of Geological and Mineral Resources., 2002, Tectonic Map of Mongolia.

Jahn, B.-M. 2004, The Central Asian Orogenic Belt and growth of the continental crust in the Phanerozoic: *Geological Society, London, Special Publications*, v. 226, no.1, p. 73-100.

Jishun, R., and Tingyu, C., 1989, Tectonic evolution of the continental lithosphere in eastern China and adjacent areas: *Journal of Southeast Asian Earth Sciences*, v. 3, no.1–4, p. 17-27.

Jong, K., Kurimoto, C., and Ruffet, G., 2009, Triassic 40Ar/39Ar ages from the Sakaigawa unit, Kii Peninsula, Japan: implications for possible merger of the Central Asian Orogenic Belt with large-scale tectonic systems of the East Asian margin: *Int J Earth Sci (Geol Rundsch)*, v. 98, no.6, p. 1529-1556.

Keller, E. A., Pinter, N., 1996, Active tectonics: Earthquakes, uplift, and landscape, 2nd ed.

Kelty, T. K., Yin, A., Dash, B., Gehrels, G. E., and A. E. Ribeiro, A. E., 2008, Detrital-zircon geochronology of Paleozoic sedimentary rocks in the Hangay–Hentey basin, north-central Mongolia: Implications for the tectonic evolution of the Mongol–Okhotsk Ocean in central Asia: *Tectonophysics*, v. 451, no.1–4, p. 290-311.

Kröner, A., Lehmann, J., Schulmann, K., Demoux, A., Lexa, O., Tomurhuu, D., Štípská, P., Liu, D., and Wingate, M. T. D., 2010, Lithostratigraphic and geochronological constraints on the evolution of the Central Asian Orogenic Belt in SW Mongolia: Early Paleozoic rifting followed by late Paleozoic accretion: *American Journal of Science*, v. 310, no. 7, p. 523-574.

Kuzmichev, A., Kröner, A., Hegner, E., Dunyi, L., and Yusheng, W., 2005, The Shishkhid ophiolite, northern Mongolia: A key to the reconstruction of a Neoproterozoic island-arc system in central Asia: *Precambrian Research*, v.138, no. 1–2, p. 125-150.

Lamb, M.A. and Badarch, G., 1997, Paleozoic sedimentary basins and volcanic-arc systems of the Asia and the Pacific Rim, International Geology Review, v. 39, p. 542-576.

Li, J. Y., 2006, Permian geodynamic setting of Northeast China and adjacent regions: closure of the Paleo-Asian Ocean and subduction of the Paleo-Pacific Plate: *Journal of Asian Earth Sciences*, v. 26, no. 3–4, p. 207-224.

Mossakovsky, A. A., Ruzhentsev, S.V., Samygin, S. G., and Kheraskova, T. N., 1994, Central Asian Fold Belt: Geodynamic evolution and formational history: *Geotectonics*, v. 27, no. 6, p. 445-474.

Şengör, A. M. C., and Natal'in, B. A., 1996, Paleotectonics of Asia: fragments of a synthesis: *in The Tectonic Evolution of Asia*, edited by Yin, A., and Harrison, M., p. 486-641.

Şengör, A. M. C., Natal'in, B. A., and Burtman, V. S., 1993, Evolution of the Altaid tectonic collage and Palaeozoic crustal growth in Eurasia: *Nature*, v. 364 no. 6435, p. 299-307.

Tapponnier, P., and Molnar, p., 1979. Active faulting and Cenozoic tectonics of the Tien Shan, Mongolia, and Baykal regions: Geophysics, v. 84, p. 3425-3459.

Tomurtogoo, O., 2002, and the Institute of Geological and Mineral Resources, A brief explanatory note to the tectonic map of Mongolia at a scale of 1:1,000,000.

Vries, M. F. W. d., Manibazar, N., and Dügerlham, S., 1996, The Vegetation of the Forest-Steppe Region of Hustain Nuruu, Mongolia: Vegetatio, v. 122, no. 2, p. 111-127.

Walker, R. T., Molor, E., Fox, M., and Bayasgalan, A., 2008, Active tectonics of an apparently aseismic region: distributed active strike-slip faulting in the Hangay Mountains of central Mongolia: *Geophysical Journal International*, v. 174, no. 3, p. 1121-1137.

Wilhem, C.,Windley, B. F., and Stampfli, G. M., 2012, The Altaids of Central Asia: A tectonic and evolutionary innovative review: *Earth-Science Reviews*, v. 113, no. 3–4, p. 303-341.

Windley, B. F., and Allen, M. B., 1993, Mongolian plateau: Evidence for a late Cenozoic mantle plume under central Asia: *Geology*, v. 21, no. 4, p. 295-298.

Windley, B. F., Alexeiev, D., Xiao, W., Kröner, A., and Badarch, G., 2007, Tectonic models for accretion of the Central Asian Orogenic Belt: *Journal of the Geological Society*, v. 164, no. 1, p. 31-47.

Xiao, W., Windley, B. F., Hao, J., and Zhai, M., 2003, Accretion leading to collision and the Permian Solonker suture, Inner Mongolia, China: Termination of the central Asian orogenic belt: *Tectonics*, v. 22, no. 6, p. 1069.

Xiao, W., Windley, B. F., Badarch, G., and Sun, S., 2004, Palaeozoic accretionary and convergent tectonics of the southern Altaids: implications for the growth of Central Asia: *Journal of the Geological Society*, v. 161, no. 3, p. 339-342.

Xu, B., Charvet, J., Chen, Y., Zhao, P., and Shi, G., 2013, Middle Paleozoic convergent orogenic belts in western Inner Mongolia (China): framework, kinematics, geochronology and implications for tectonic evolution of the Central Asian Orogenic Belt: *Gondwana Research*, v. 23, no.4, p. 1342-1364.

Yin, A., 2006, Cenozoic tectonic evolution of the Himalayan orogen as constrained by along strike variation of structural geometry, exhumation history, and foreland sedimentation: *Earth-Science Reviews*, v. 76, no. 1-2, p. 1-131.

Zorin, Y. A., 1999, Geodynamics of the western part of the Mongolia–Okhotsk collisional belt, Trans-Baikal region (Russia) and Mongolia: *Tectonophysics*, v. 306, no. 1, p. 33-56.

Zorin, Y. A., Belichenko, V. G., Turutanov, E. K., Kozhevnikov, V. M., Ruzhentsev, S. V., Dergunov, A. B., Filippova, I. B., Tomurtogoo, O., Arvisbaatar, N., Bayasgalan, T., Biambaa, C., and Khosbayar, P.,1993, The South Siberia-Central Mongolia transect: *Tectonophysics*, v. 225, no. 4, p. 361-378.